Extreme geochemical variability through the dunitic transition zone of the Oman ophiolite: Implications for melt/fluid-rock reactions at Moho level beneath oceanic spreading centers

Rospabé Mathieu [1, *], Benoit Mathieu [1], Ceuleneer Georges [1], Hodel Florent [1, 2], Kaczmarek Mary-Alix [1, 3]

[1] Univ Toulouse, CNRS, IRD, GET,Observ Midi Pyrenees, 14 Ave E Belin, F-31400 Toulouse, France.
[2] Univ Sa Paulo, Inst Astron Geofis & Ciencias Atmosfer, BR-05508900 Sao Paulo, Brazil.
[3] Univ Lausanne, Inst Earth Sci, CH-1015 Lausanne, Switzerland.

* Corresponding author : Mathieu Rospabé, email address : mathieu.rospabe@get.omp.eu

Abstract :

The Maqsad area in the Oman ophiolite exposes a >300 m thick dunitic mantle-crust transition zone (DTZ) that developed above a mantle diapir. The Maqsad DTZ is primarily made of "pure" dunites (olivine with scattered chromite and chromite seams) and "impregnated" dunites, which exhibit a significant lithological variability, including various kinds of clinopyroxene-, plagioclase-, orthopyroxene-, amphibole (hornblende/pargasite)-bearing dunites. These minerals are interstitial between olivine grains and their variable abundance and distribution suggest that they crystallized from a percolating melt. Generally studied through in-situ mineral characterization, the whole rock composition of dunites is poorly documented. This study reports on whole rock and minerals major and trace element contents on 79 pure to variably impregnated dunites collected systematically along cross sections from the base to the top of the DTZ. In spite of its high degree of depletion, the olivine matrix is selectively enriched in the most incompatible trace elements such as LREE, HFSE, Th, U, Rb and Ba. These data support the view that this enrichment has been acquired early in the magmatic evolution of the DTZ, during the dunitization process itself. The dissolution of orthopyroxene from mantle harzburgites enhanced by the involvement of hydrothermal fluids produced low amounts of melts enriched in silica and in some trace elements that re-equilibrated with the olivine matrix. This pristine signature of the DTZ dunite was eventually variably altered by percolation of melts with a Mid-Ocean Ridge Basalt (MORB) affinity but displaying a wide spectrum of composition attributable to evolution by fractional crystallization and hybridization with the silica enriched, hydrated melts. The olivine matrix has been partially or fully re-equilibrated with these melts, smoothing the early strong concave-upward REE pattern in dunite. The chemical variability in the interstitial minerals bears witness of the percolation of MORB, issued from the mantle decompression melting, variably hybridized with melt batches produced within the DTZ by melt-rock reaction and poorly homogenized before reaching the lower crust. Our results lead to the conclusion that pure and impregnated dunites are end-members that recorded different stages of the same initial igneous processes: pure dunites are residues left after extraction of a percolating melt while impregnated dunites

correspond to a stage frozen before complete melt extraction. Therefore dunites trace elements contents allow deciphering the multi-stage processes that led to their formation at the mantle-crust transition zone.

50

1. Introduction

The boundary between the Earth mantle and the oceanic crust is underlined by a dunitic horizon in most ophiolites worldwide, regardless the tectonic setting in which they evolved (mid-ocean ridges vs. supra-subduction zone) (e.g. Moores and Vine, 1971; Prinzhofer et al., 1980; Boudier and Coleman, 1981; Quick, 1981; Jan and Howie, 1981; Kelemen et al., 1997a; Bédard and Hébert, 1998; Ceuleneer and le Sueur, 2008; Bouilhol et al., 2009). Since dunites are observed in present-day oceans in different tectonic settings, associated to mantle harzburgites and to troctolitic-gabbroic veins and sills like in the dunitic mantle-crust transition zone (DTZ) (e.g. Arai and Matsukage, 1996; Dick and Natland, 1996; Parkinson and Pearce, 1998; Savov et al., 2005; Godard et al., 2008), it is reasonable to suppose that ophiolitic DTZ formed prior to the intra-oceanic thrusting leading to obduction.

A residual origin for dunites after very high (>40%) degrees of partial melting of the mantle (Green and Ringwood, 1967) requires unrealistic thermal regimes, at least in the modern Earth and in oceanic spreading contexts (Herzberg et al., 1983). Alternatively, dunite may result from the accumulation of olivine grains issued from fractional crystallization from a melt sufficiently rich in Mg to remain during a significant time in the fractionation field of olivine alone (+/- spinel) (Bowen, 1915; O'Hara, 1965; Elthon, 1979). Finally, dunite may be replacive after interaction ("reactional melting") between melts and peridotite in dry (Bowen, 1927; Berger and Vannier, 1984) or hydrated systems (Bowen and Tuttle, 1949). The interaction between harzburgite and a melt undersatured in silica accounts for the formation of dunite through the dissolution of pyroxenes, leading to the enrichment in silica of the melt with concomitant crystallization of olivine (Dick, 1977; Quick, 1981; Kelemen, 1990; Kelemen et al., 1992). Petrological evolutions across a densely sampled cross section along a

75 330 m thick DTZ of the Oman ophiolite revealed that the DTZ does essentially but not

76 exclusively derive from melt-peridotite interaction, its shallowest part (topmost 50 m)

77 showing fractional crystallization trends (Abily and Ceuleneer, 2013).

78

79 In the melt-rock reaction model, it was proposed that reactional melting and orthopyroxene

80 consumption leads to high intergranular permeability enhancing the efficiency of melt

81 extraction from the mantle (Ortoleva et al., 1987; Daines and Kohlstedt, 1994; Kelemen et al.,

82 1995a; Kelemen et al., 1997b). In this way, the DTZ appears to be a reactive interface where

83 melts are focused, transformed and potentially accumulated, then distributed beneath the mid-

84 ocean ridge. Crystallization associated to melt migration through the mantle-crust transition

85 zone accounts for the wide diversity of lithological facies observed in the DTZ. Dunites

86 evolve from "pure dunites", i.e. compacted at very high temperature when complete melt

87 extraction occurred, to "impregnated dunites", highly refertilized before incipient cooling and

88 that potentially leads in extreme cases to the formation of hybrid olivine-rich troctolites or

89 plagioclase-bearing wehrlites (e.g. Arai and Matsukage, 1996; Abily and Ceuleneer, 2013;

90 Sanfilippo and Tribuzio, 2013a). Although interstitial minerals in ophiolites or abyssal DTZ

91 are regularly found in equilibrium with melts that fed the overlying crust (e.g. Drouin et al.,

92 2009; Ghosh et al., 2014; Nicolle et al., 2016), the Oman ophiolite DTZ was also percolated

93 by melts with more exotic compositions (Koga et al., 2001) that, for a part of them, may be

94 attributable to hybridization with a hydrothermal fluid component (Rospabé et al., 2017).

95 Especially the presence of orthopyroxene, amphibole, garnet and diopsides both interstitially

96 between olivine grains and in inclusion in chromite calls for early, high temperature,

97 hydration of the DTZ. In this frame, to define the origin of the DTZ has direct implications on

98 melt generation, transfer and evolution from the mantle to the crust, as well as on the deep

99 hydrothermal circulations that may influence both the chemical exchanges and the thermal

100   structure of the oceanic lithosphere.

101

102   Most geochemists use the trace element contents of interstitial clinopyroxene and plagioclase

103   (if any) scattered in dunites to build petrological scenario (e.g. Kelemen et al., 1995a; Nicolle

104   et al., 2016; Akizawa et al., 2016a). However, it concerns actually the genesis of

105   crystallization products from melt fractions that travelled through the dunites, which might be

106   risky to extrapolate to the genesis of the dunitic matrix itself. Very few whole rock analysis or

107   olivine trace element contents are available due to their very low content in olivine. The

108   sporadic studies providing trace elements data on dunite show that re-equilibration processes

109   occurred between the olivine matrix, selectively enriched in some trace elements, and the

110   melts percolating interstitially between olivine grains (e.g. Godard et al., 2000; Gerbert-

111   Gaillard, 2002; Sanfilippo et al., 2014, 2017).

112

113   To better constrain the processes leading to the formation of both pure and impregnated

114   dunitic products constituting the DTZ as well as to their chemical signature, we combined

115   major and trace elements in whole rock and in mineral phases for 79 samples of dunite from

116   the Oman ophiolite mantle-crust transition zone. We show that the important chemical

117   variability recorded by the dunites at Moho level is issued from a combination of harzburgite

118   dunitization, re-equilibration associated to melt percolation, and refertilization from unmixed

119   and contrasted MORB-derived melt batches variably hybridized with hydrous fluids.

120

121   **2. Geological background**

122   *2.1. Geology of the Oman ophiolite*

123   The Oman ophiolite exposes a 30.000 km^2 remnant of the Tethyan Ocean. Its creation

124   occurred ~95-97 million years ago (Tilton et al., 1981; Tippit et al., 1981; Rioux et al., 2012)

125   and was directly followed by an oceanic detachment close to the ridge axis that eventually led

126   to its obduction on the Arabian margin (Lanphere, 1981; Boudier et al., 1985; Boudier et al.,

127   1988; Montigny et al., 1988). The synoptic mapping of mafic-ultramafic dykes cropping out

128   in the mantle section (Python and Ceuleneer, 2003; Python et al., 2008) revealed that two

129   main magmatic suites contributed to the igneous evolution of the ophiolite: (1) a MORB suite

130   mostly present in the southeastern massifs of the ophiolite (Nakhl, Sumail and Wadi Tayin)

131   and in some restricted areas in the north, and (2) a more widespread depleted-andesitic type

132   attributed either to subduction or to hydrated re-melting of the shallow lithosphere during

133   spreading (Pearce et al., 1981; Benoit et al., 1999; Python and Ceuleneer, 2003; Yamasaki et

134   al., 2006; MacLeod et al., 2013) (Fig. 1a).

135

136   Along the Oman ophiolite, spatially constrained vertical flow structures within the mantle

137   section were interpreted as former asthenospheric diapirs distributed along the oceanic ridge

138   (Ceuleneer et al., 1988; Nicolas et al., 1988; Jousselin et al., 1998; Nicolas et al., 2000). The

139   Sumail massif, focus of the present study, exposes in the Maqsad area a well preserved paleo

140   mantle diapir and its associated N130 paleo-spreading center (Ceuleneer, 1986; Ceuleneer et

141   al., 1988; Ceuleneer, 1991; Jousselin et al., 1998). This structure is located in the central part

142   of the largest (80 × 25 km) MORB district of Oman (Python and Ceuleneer, 2003) (Fig. 1).

143   The MORB affinity has been evidenced by the crystallization sequence and confirmed by

144   trace elements and isotopic data on both mantle and crustal rocks (Benoit et al., 1996;

145   Ceuleneer et al., 1996; Godard et al., 2000; Koga et al., 2001; Godard et al., 2003; Clénet et

146   al., 2010).

147

148   *2.2. The dunitic transition zone around the Maqsad diapir*

149   The thickness of the DTZ reaches 300 to 350 m above the central part of the Maqsad mantle

150 diapir (Rabinowicz et al., 1987; Boudier and Nicolas, 1995; Jousselin and Nicolas, 2000;

151 Abily and Ceuleneer, 2013) and thins progressively off-axis due to tectonic transposition by

152 mantle plastic flow as it diverges from the diapir (Ceuleneer, 1991). In this area the DTZ was

153 mainly described as the uppermost part of the mantle, modified after complete orthopyroxene

154 consumption resulting from MORB-peridotite interaction (Godard et al., 2000; Gerbert-

155 Gaillard, 2002), while its upper part (top most ~50 m) displays all the characteristic of

156 cumulates (Abily and Ceuleneer, 2013). The interstitial plagioclase and clinopyroxene located

157 between olivine grains exhibit chemical signature in good agreement with a fractionation

158 from a percolating MORB (Koga et al., 2001; Abily and Ceuleneer, 2013; Nicolle et al.,

159 2016). It was also recently evidenced that some horizons of the DTZ contain interstitial

160 orthopyroxene and pargasite that support the percolation of a hybrid liquid, i.e. a blend of

161 variably evolved MORB and of hydrous silica-rich liquids (Rospabé et al., 2017). The

162 ubiquitous occurrence of hydrothermal diopside and grossular, both in interstitial position

163 between olivine grains and enclosed in disseminated chromite together with orthopyroxene,

164 pargasite, biotite and aspidolite, suggests them as primary high temperature features and

165 further challenges the pure igneous origin of the DTZ. According to our observations, they are

166 not systematically associated to cracks affecting chromite grain, as would be expected if they

167 were low temperature alteration products resulting from serpentinization and Ca-rich

168 metasomatism having affected mafic and ultramafic rocks (e.g. Palandri and Reed, 2004;

169 Python et al., 2011; Akizawa et al., 2016b) (see also Tamura et al., 2014). The possible

170 involvement of high temperature hydrothermal fluids during the magmatic stage that edified

171 the DTZ allows reconsidering the former hypothesis of a hydrothermal origin for dunites,

172 originally proposed by Bowen and Tuttle (1949).

173

174 **3. Methods**

175   *3.1. Sampling strategy*

176   The Sumail massif was slightly tilted during the Miocene uplift of the Djebel Akhdar. Its

177   regional dip does not exceed 10° to the SE. For this reason, to perform sampling along

178   distributed cross sections is a straightforward way to reconstruct the three-dimensional

179   structuration of the DTZ around the Maqsad diapir and its associated paleo-ridge axis. In this

180   study we report on whole rock and mineral major elements and whole rock trace elements for

181   79 samples, and on interstitial clinopyroxenes trace elements for 11 impregnated dunites.

182   Samples were collected systematically every 10 to 20 m vertically along four cross sections

183   (Fig. 1b). Their location and mineral contents are presented in Table 1.

184

185   *3.2. Analytical methods*

186   *In situ* mineral major element concentrations were acquired by electron microprobe using a

187   Cameca SX 100 (Microsonde Ouest, Brest, France) and a Cameca SXFive (Centre de

188   MicroCaractérisation Raimond Castaing, Toulouse, France) with a 20 kV accelerating

189   voltage, a beam current of 20 nA, an electron beam diameter of 1 μm for all analyses and a

190   counting time of 10 s on peak for each element and 5 s on backgrounds on both sides of the

191   peak. *In situ* clinopyroxene trace element concentrations were obtained by laser ablation-

192   inductively coupled plasma-mass spectrometry (LA-ICP-MS) at the Institute of Earth

193   Sciences, University of Lausanne (Switzerland). We used a NewWave UP-193 ArF

194   Excimer based laser ablation system coupled with a Thermo Scientific™ ELEMENT XR™

195   high resolution ICP-MS. Spot size ranged between 75 and 100 μm and operating conditions

196   were a 20 Hz pulse rate and an energy density of 6.0 J/cm^2. The SRM612 NIST was used as

197   external standard following the values proposed by Jochum et al. (2011) and ^{29}Si was used as

198   internal standard.

199

200   Whole rock major element concentrations were obtained by X-ray Fluorescence Spectrometry

201   at the Central Analytical Facilities, Stellenbosch University (South Africa). Whole rock trace

202   element concentrations were acquired on a Thermo Scientific™ ELEMENT XR™ HR-ICP-

203   MS at the Géosciences Environnement Toulouse laboratory (Observatoire Midi-Pyrénées),

204   Université of Toulouse III. The sample preparation consisted in a HF-HClO$_4$ digestion

205   procedure (Yokoyama et al., 1999) combined with a thulium addition (Barrat et al., 1996).

206   The concentrations in Li and Large Ion Lithophile Elements (LILE; Rb, Sr, Cs and Ba) and of

207   most of transition elements (Cr, Mn, Co, Ni, Cu, Zn) and Ga were acquired after a direct

208   digestion/dilution method. Sc, V, Rare Earth Elements (REE) and Y, High Field Strength

209   Elements (HFSE; Zr, Hf, Nb, Ta, Ti) and U, Th and Pb contents were determined after the

210   double coprecipitation procedure detailed in Rospabé et al. (2018). BHVO-2 was used as

211   calibrator following the values proposed by Barrat et al. (2012). The yield was monitored and

212   concentrations calculated using the Tm anomaly appearing in the samples REE pattern (Barrat

213   et al., 1996). The international rock standards UB-N (serpentinite) and DTS-2B (dunite) were

214   analysed as unknown during the course of this study. They are given in Appendix A together

215   with the samples major and trace element compositions.

216

4. Lithological diversity in the Maqsad DTZ

218   Olivines exhibit a recrystallized equigranular mosaic texture with frequent triple junctions at

219   120° (Fig. 2a). Its average grain size is about 1 mm. All samples are affected to some degree

220   by serpentinization, which ranges from about 30 to 60%. Submillimeter round-shaped

221   chromite grains are interstitial between olivine grains. They are generally disseminated but

222   chromite schlierens occur in some samples. Small grains of clinopyroxene are also frequently

223   observed at olivine triple junctions or along the olivine grain rims, with a grain size no larger

224   than few tens of microns. Samples with less than 0.5% of clinopyroxene are considered as

225   "pure dunites" (38 samples).

226

227   The remaining 41 samples contain well-developed oikocrystic of clinopyroxene and/or other

228   interstitial minerals. These interstitial phases are classically interpreted as crystallization

229   products fractionated from a melt that percolated through the dunitic matrix and are referred

230   to as "impregnated dunites" (Benn et al., 1988; Boudier and Nicolas, 1995; Koga et al., 2001;

231   Abily and Ceuleneer, 2013). Two contrasted clinopyroxene compositions are observed; one

232   consistent with an igneous origin and the other one calling for crystallization from

233   hydrothermal fluids or water-rich melts (Python et al., 2007; Rospabé et al., 2017).

234   Accordingly, we use "clinopyroxene" and "diopside" to distinguish clinopyroxene with

235   igneous and hydrothermal origin respectively. Clinopyroxene is the most common

236   impregnating phase (14 samples are cpx-bearing dunites). Its texture changes with its modal

237   abundance, from small interstitial at olivine grains boundaries (up to hundreds microns width

238   in size) to oikocrystic crystals (millimeter to up to centimetre in size) (Fig. 2b). Smaller

239   interstitial diopsides are also sometimes observed both in pure and impregnated dunites,

240   showing different texture and chemical content than the clinopyroxene oikocrysts (Fig. 2c).

241   Plagioclase appears as a well-developed interstitial intercumulus phase, generally as

242   oikocrysts (Fig. 2d), and is regularly associated to clinopyroxene, characterizing the pl/cpx-

243   bearing dunites (14 samples). Plagioclase-bearing cpx-free dunites are rarely observed (one

244   sample only). Plagioclase/olivine contacts are also regularly underlined by a clinopyroxene

245   corona. In addition to clinopyroxene and plagioclase, the dunites collected in the DTZ from

246   the Maqsad area show orthopyroxene oikocrysts in pl/cpx-bearing dunites (7 samples) (Fig.

247   2e), and amphibole, observed as subhedral crystals in few samples with no preference to the

248   other minerals present (7 samples) (Fig. 2f). Interstitial subhedral grossular garnet was

249   observed in 12 impregnated dunites (Rospabé et al., 2017). All these interstitial minerals are

250 also present as round-shaped primary inclusions in chromite grains together with micas

251 (phlogopite and aspidolite), the latter being never observed interstitially within the dunitic

252 matrix.

253

254 **5. Results**

255 *5.1. Whole rock major and minor elements*

256 The dunites from the DTZ plot above the mantle fractionation array in the MgO/SiO_2 vs.

257 Al_2O_3/SiO_2 diagram (Fig. 3a). Pure dunites and slightly impregnated ones (<5% of cpx or cpx

258 + pl) exhibit a more refractory characteristic than the most depleted harzburgites from the

259 mantle section with higher MgO/SiO_2 (>1.1) and lower Al_2O_3/SiO_2 (<0.02) ratios.

260 Impregnated samples are generally characterized by a progressive decrease of MgO/SiO_2 and

261 an increase of Al_2O_3/SiO_2 that reflects an increasing amount of clinopyroxene and

262 plagioclase. The loss on ignition (LOI) is comprised between 6.9 and 10.9 wt.% for pure

263 dunites and 4.7 and 10.8 wt.% for impregnated dunites, and reflects primarily the degree of

264 serpentinization that is similar in both dunite types (Appendix A). The variation of FeO and

265 MgO in pure and slightly impregnated dunites perfectly mimics the stoichiometric variation

266 of the olivine Fe-Mg composition (FeO + MgO = 66.67 in mol%) while other higher

267 impregnated samples contain a lower MgO content similar to mantle harzburgites (mainly

268 ~43-47 wt.%) (Fig. 3b).

269

270 Low CaO and Al_2O_3 also characterize the pure and slightly impregnated dunites with

271 concentrations lower than 1 wt.% (Fig. 3c). The higher CaO and Al_2O_3 contents are strongly

272 correlated to the abundance of impregnating minerals. The modal proportion of clinopyroxene

273 controls the CaO content that increases fast with increasing amount of cpx ($Al_2O_3/CaO<1$ in

274 cpx-bearing dunites) while plagioclase and amphibole exert the main control on the Al_2O_3

275   content in other impregnated dunites ($Al_2O_3/CaO > 1$).

276

277   In pure dunites the Mg# ($100 \times$ molar $Mg/(Mg + Fe_{total})$) is more variable (from 86 to 92.3,

278   except a pure dunite containing schlierens of chromites with a whole rock Mg# = 83.4) than

279   in impregnated dunites (from 87.2 to 90.9) and peridotites from the mantle section (from 89.8

280   to 91.6). The dunites from the DTZ also display a much more variable Ni (1207-2870 µg/g)

281   and a higher Co (110-155 µg/g) contents than mantle peridotites (Ni = 1747-2671 µg/g; Co =

282   95-122 µg/g) (Fig. 3d and 3e). These compositions are not clearly related to the degree of

283   impregnation minerals with high Ni and Co concentrations also observed in the most

284   impregnated samples.

285

286   *5.2 Mineral major elements*

287   The Fo in olivine ($100 \times$ molar $Mg/(Mg + Fe_{total})$) in dunites from the DTZ generally

288   decreases from 92.5 to 87.8 concomitantly with the NiO content (0.45 to 0.19 wt.%) (Fig. 4a).

289   This compositional range is broader than in the peridotites from the mantle section

290   (89.5<Fo<92.1; 0.25<NiO<0.53 wt.%). The CaO content in olivine, mainly <0.05 wt.% in

291   mantle harzburgites, reaches 0.32 wt.% in the DTZ. Higher CaO values are generally

292   observed in olivine grains from pure dunites, also displaying the lower Fo and NiO contents

293   (Fig. 4b), and may consequently not be attributed to re-equilibration with other CaO-rich

294   minerals. Fo in olivine and Mg# in whole rocks are highly correlated (Fig. 4c).

295

296   The Cr# ($100 \times$ molar $Cr/(Cr + Al)$) variation range in chromite is more restricted in dunites

297   from the DTZ (43.3-63.4) than in harzburgites from the mantle section (20.6-70). Cr# gently

298   decreases with the Fo and progressively shifts from the olivine-spinel mantle array (OSMA)

299   (Arai, 1987, 1994) (Fig. 4d). Mg# ($100 \times$ molar $Mg/(Mg + Fe^{2+})$) in chromite is quite similar

300 between the different types of dunite (43.3-63.4) while the TiO_2 content is on the contrary

301 much more variable depending on the host lithological facies (Fig. 4e), being lower (0.20-

302 0.60 wt.%) in pure dunites than in impregnated ones (mainly comprised between 0.15 and 0.9

303 wt.% and occasionally reaching 1.3 wt.%). On the contrary YFe^{3+} ($100 \times$ molar Fe^{3+}/(Cr + Al

304 + Fe^{3+})) is slightly higher in chromite from the pure dunites (Appendix B).

305

306 Minute clinopyroxenes were observed at the triple junction of olivine grains in what we

307 defined as pure dunites. They exhibit a variable Mg# (86.9-94.2) and a CaO content

308 exceeding 24.5 wt.% that contrast with the clinopyroxene oikocrysts from the impregnated

309 dunites (Mg# = 89.6-92.9; CaO = 21.1-24.8 wt.%) (Appendix B). All the clinopyroxenes

310 display a wide variation range in TiO_2 (0.16-0.71 wt.%) (Fig. 4f), Cr_2O_3 (0.79-1.32 wt.%) and

311 Al_2O_3 (2.6-4.9 wt.%) (Appendix B). Zoning was observed in few clinopyroxenes only, with

312 the concomitant increase of Mg#, SiO_2 and TiO_2 together with the decrease of Al_2O_3 and

313 Cr_2O_3 from the core to the rim. Small interstitial diopside composition ranges between

314 igneous and hydrothermal end-members, with higher Mg# and lower TiO_2 (Fig. 4f), Cr_2O_3

315 and Al_2O_3 contents (see also Rospabé et al., 2017).

316

317 Oikocrystic orthopyroxene grains observed in interstitial position in dunites present a high

318 TiO_2 content (0.15-0.23 wt.%), specific to the dunites from the Maqsad area (Rospabé et al.,

319 2017) (Appendix B). They display Mg# and Al_2O_3 contents varying from 88.8 to 90.8 and

320 1.15 to 2.22 wt.% respectively. As clinopyroxene, orthopyroxene rarely exhibits zoned

321 compositions with the increase of SiO_2 concomitantly to the decrease of Al_2O_3, and Cr_2O_3

322 from the core to the rim. Mg# is quite variable as MgO and FeO both increase with SiO_2.

323

324 Plagioclase was not systematically analysed in each pl-bearing dunites due to its higher

325 degree of alteration than other phases. It presents rather primitive compositions in

326 (opx/)pl/cpx-bearing dunites (An (100 × molar Ca/(Ca + Na + K)) = 86.3-90.1) while being

327 more evolved in one amphibole/pl/cpx-bearing dunite (An = 74.6) (Appendix B).

328

329 Interstitial amphiboles in the studied samples are pargasites, pargasitic- or edenitic-

330 hornblende. They display Mg# ranging from 85.7 to 91.4 and extremely variable Al_2O_3 (11.0-

331 16.3 wt.%), Na_2O (1.98-3.75 wt.%), TiO_2 (0.02-1.24 wt.%) and Cr_2O_3 (0.01 to 1.81 wt.%)

332 contents (Appendix B).

333

334 *5.3. Whole rock trace elements*

335 The dunites from the DTZ exhibit variable trace element compositions (Appendix A). Pure

336 dunites are highly depleted in lithophile trace elements with concentrations below both the

337 chondritic and the Primitive Mantle (PM) values (mostly comprised between 0.001 and 0.1

338 times the PM concentrations). Pure dunites are characterized by U- or V-shape REE

339 chondrite-normalized patterns (Fig. 5a), reflecting the major MREE (Sm, Eu and Gd)

340 depletion relative to LREE (La_{CN}/Sm_{CN} <3.76; 1.9 in average) and HREE (0.04< Gd_{CN}/Yb_{CN}

341 <0.28). We define the U- or V-shape appellation depending on the presence or absence of

342 negative Eu anomaly. The $(Eu/Eu*)_{CN}$ ratio ranges between 0.22 and 1 in 29 samples, while 9

343 samples exhibit a positive Eu anomaly with $(Eu/Eu*)_{CN}$ <2.4 ($(Eu/Eu*)_N = Eu_{CN}/\sqrt{(Sm_{CN} \times}$

344 $Gd_{CN})$). Pure dunites display relative homogeneous HREE concentrations (Yb_{CN} = 0.10-0.24)

345 in comparison to more variable MREE (0.005< Gd_{CN} <0.059; 0.004< Sm_{CN} <0.065) and

346 especially LREE (0.004< La_{CN} <0.17). The depletion from HREE to MREE is not linear with

347 several samples exhibiting instead concave-upward patterns with a progressive Gd_{CN}/Dy_{CN}

348 increase for a constant Er_{CN}/Yb_{CN}. Pure dunites U-shaped PM-normalized multi-elements

349 patterns exhibit significant enrichments in LILE, Th, U, Nb and Ta relative to LREE

350   (Rb_{PMN}/La_{PMN} = 1.5-85; Th_{PMN}/La_{PMN} = 0.7-5.3) and strong Pb and Sr positive anomalies

351   similar to mantle peridotites (2.19< Pb_{PMN}/Ce_{PMN} <1294) (Fig. 5b). Zr and Hf are generally

352   enriched relative to MREE (Zr_{PMN}/Sm_{PMN} = 0.6-27; 2.9 in average) as well as Ti that displays

353   a strong positive anomaly (1.3< Ti_{PMN}/Gd_{PMN} <76).

354

355   Cpx-bearing dunites exhibit variable REE and multi-element patterns partly attributable to

356   variations in the interstitial clinopyroxene content. Slightly impregnated ones (<5% cpx)

357   exhibit linear LREE-depleted or slightly concave-upward REE patterns (La_{CN}/Yb_{CN} = 0.06-

358   0.97) with similar HREE concentrations (Yb_{CN} = 0.12-0.29) and more restricted LREE and

359   MREE variation ranges (La_{CN} = 0.01-0.23; Gd_{CN} = 0.02-0.12) than pure dunites (Fig. 5c).

360   Dunites containing a higher amount of clinopyroxene have higher HREE contents (Yb_{CN} =

361   0.56-0.83). They exhibit clear convex-upward patterns with a nearly flat slope of the HREE

362   segment (Gd_{CN}/Yb_{CN} = 0.74-0.85) followed by a progressive depletion from MREE to LREE

363   (La_{CN}/Sm_{CN} = 0.06-0.09). It is worth noting that the cpx-bearing dunites display La and Ce

364   contents within the variation range of pure dunite (La_{CN} = 0.01-0.23). This observation may

365   be extended to other incompatible trace elements like Th, U, HFSE that are not more

366   concentrated in cpx-bearing dunites than in pure dunites, excepting one sample that displays

367   spectacular HFSE positive anomalies (Fig. 5d). Cpx-bearing dunites exhibit similar

368   enrichment in LILE relative to LREE and the same strong positive Pb and Sr anomalies than

369   in pure dunites. The positive Ti anomaly observed for the slightly impregnated samples

370   disappears for the more impregnated ones in which the Ti content is buffered around 0.25

371   times the PM value.

372

373   The pl-bearing dunite displays a W-shaped REE pattern with strong depletion in MREE

374   (Sm_{CN} = 0.005; Gd_{CN} = 0.003) relative to LREE (La_{CN}/Sm_{CN} = 4.3) and HREE (Gd_{CN}/Yb_{CN} =

375 0.002) bordering a strong positive Eu anomaly (($Eu/Eu^*)_{CN}$ = 54) (Fig. 5e). Other pl/cpx-

376 bearing chondrite-normalized REE patterns evolve from concave-upward to convex upward

377 with the increasing amount of clinopyroxene. This evolution is accounted by a progressive

378 decrease of the HREE segment slope (Gd_{CN}/Yb_{CN} from 0.17 to 0.63). They are also

379 characterized, in regard to pure and cpx-bearing dunites, by higher Li and Rb contents, a

380 higher range of Cs, a well depletion in their Th and U contents, and a slighter positive Pb

381 anomaly (Fig. 5f).

382

383 Opx/pl/cpx-bearing dunites and amphibole-bearing dunites (± opx, pl and cpx) have REE

384 contents similar to pl/cpx-bearing dunites with patterns intermediate between highly

385 impregnated pl-bearing and cpx-bearing dunites (Fig. 5g). They also display similar PM-

386 normalized multi-elements patterns than pl/cpx-bearing dunites, with Th, U, and with few

387 exceptions Nb and Ta contents similar to LREE (averaged Th_{PMN}/La_{PMN} = 0.9) (Fig. 5h).

388

389 *5.4. Clinopyroxene minor and trace elements*

390 Trace elements concentrations were obtained for unzoned crystals of clinopyroxene in 11

391 impregnated dunites (2 cpx-bearing, 6 pl/cpx-bearing, 3 opx/pl/cpx-bearing, and 1

392 amph/opx/pl/cpx-bearing). Their composition is homogeneous within a given sample. In

393 clinopyroxenes, lower trace elements contents are observed in the amph/opx/pl/cpx-bearing

394 dunite while higher contents much characterize cpx-bearing dunites; clinopyroxenes in

395 (opx/)pl/cpx-bearing dunites display both low and high trace elements concentrations.

396 Regarding the chondrite-normalized REE patterns, all the clinopyroxenes are depleted in

397 LREE relative to MREE (La_{CN}/Sm_{CN} = 0.03-0.32) and the slope in HREE is highly variable,

398 from strongly positive to moderately negative (Gd_{CN}/Yb_{CN} = 0.61-2.28) (Fig. 6a). The most

399 LREE-depleted patterns are rather observed in (amph/)opx/pl/cpx-bearing dunites whatever

400   the REE concentrations, while the less depleted ones are observed in cpx-bearing dunites.

401   Negative anomalies in Nb and Ta (Nb_{PMN}/La_{PMN} = 0.08-1) relative to LREE and in Zr and Hf

402   relative to MREE (Zr_{PMN}/Sm_{PMN} = 0.14-0.43) are systematically observed whatever the host

403   lithology (Fig. 6b). With few exceptions, negative anomalies in Pb and Sr relative to LREE-

404   MREE are also observed as well as in Ti for the most enriched clinopyroxenes.

405

406   **6. Discussion**

407   The dunitic transition zone from the Maqsad area exposes various types of dunites,

408   characterized from their mineralogical content (Boudier and Nicolas, 1995; Koga et al., 2001;

409   Abily and Ceuleneer, 2013; Rospabé et al., 2017) and from their geochemical diversity within

410   each lithological facies. Previous studies proposed different processes to explain the

411   formation of pure and impregnated dunites and/or their geochemical signature: (1)

412   serpentinization or weathering, (2) fractional crystallization and accumulation of olivine and

413   other minerals, (3) melt-rock reactions comprising harzburgite reactional melting and re-

414   equilibration related to melt percolation and, (4) refertilization associated to melt transport. In

415   the next sections we will discuss the relative influence of each process in regard to the

416   geochemical variations revealed by our study, then we will propose a more general model for

417   the Maqsad DTZ genesis.

418

419   *6.1. Serpentinization or secondary weathering effects*

420   The dunites are partly serpentinized with a serpentine abundance of about 40 to 50% in

421   average, according to thin sections observation and loss of ignition (LOI) values.

422   Serpentinization is known to be nearly isochemical regarding the bulk rock major element

423   concentrations (e.g. Coleman and Keith, 1971; Deschamps et al., 2013). In our samples, the

424   LOI is not or poorly correlated with any major element contents attesting that the

425 serpentinization did not extensively affect bulk rock major element concentrations (see also

426 Rospabé, 2018). More specifically, the samples plot above the terrestrial array in the

427 MgO/SiO$_2$ vs. Al$_2$O$_3$/SiO$_2$ diagram (Fig. 3a) and do not show any evidence for MgO loss or

428 SiO$_2$ enrichment as reported in pervasively serpentinized abyssal peridotites or talc-bearing

429 serpentinites (Snow and Dick, 1995; Bach et al., 2004; Paulick et al., 2006; Boschi et al.,

430 2008; Malvoisin, 2015). The perfect consistency between the Fo in olivine and the Mg# in

431 whole rock (Fig. 4c) further demonstrates the absence of influence of serpentinization on the

432 bulk dunite major element compositions.

433

434 Regarding trace elements, with few exceptions, the La content is strongly correlated to the Th

435 content, in both pure and impregnated dunites (Fig. 7a). The Th, as well as HFSE, are

436 immobile during post-magmatic aqueous alteration (You et al., 1996; Kogiso et al., 1997;

437 Niu, 2004; Paulick et al., 2006). Thus, correlated enrichments of La with Th testify that LREE

438 enrichments derived from magmatic processes, as seen in mantle harzburgites from the

439 Sumail massif (Godard et al., 2000; Gerbert-Gaillard, 2002). A poorer but significant

440 correlation exists between HFSE (Zr, Hf, Nb, Ta) and U contents on one hand and Th and

441 LREE contents on the other (Fig. 7b, c and d). Rb and Ba seem to be vaguely correlated to

442 HFSE in pure dunites (especially to Zr and Hf) as well as to Th (Fig. 7e and f) and thus were

443 probably enriched during an initial igneous stage before being potentially affected again

444 during secondary weathering processes. Other LILE, such as Sr, and Pb contents are not

445 correlated to the LOI but the absence of correlation with Th suggests that their enrichment

446 could be related to a secondary alteration/serpentinization processes post-dating the igneous

447 history. This is confirmed by the fact that all the dunitic bulk rock analyses from the DTZ

448 exhibit strong positive Sr and Pb anomalies, while interstitial igneous clinopyroxenes exhibit

449 the opposite negative Sr and Pb anomalies. These trace element evolutions in regard to

450   immobile elements have been already described in Oman ophiolite mantle harzburgites

451   (Gerbert-Gaillard, 2002). The co-variations of Th, U, LREE and HFSE at least may thus be

452   interpreted in the framework of igneous processes.

453

454   *6.2. Cumulative origin*

455   A cumulative origin for dunites (Bowen, 1915; Bowen and Tuttle, 1949; O'Hara, 1965;

456   Elthon, 1979) implies to preserve a high-Mg parental melt in the crystallization field of the

457   single olivine (+/- spinel) during differentiation. This is quite problematic to account for thick

458   layers (several hundred meters or large bodies of dunites), and the production of such high

459   temperature melts is inconsistent with the inferred thermal conditions in the present day Earth

460   interior (Verhoogen, 1954; McKenzie and Bickle, 1988; Tilley et al., 2007). However, it was

461   proposed that the shallowest part of the Maqsad DTZ, where both Fo and NiO in olivine

462   decrease together upsection, was generated by olivine crystallization and accumulation while

463   the main part of the DTZ was a residue of reaction melting (Abily and Ceuleneer, 2013).

464

465   Dunites from the Maqsad DTZ exhibit Ni and Co contents that are much closer to the mantle

466   peridotites compositions (Fig. 3d and 3e) than to the most primitive troctolite cumulates

467   cropping out within the mantle harzburgitic section in the Maqsad area (Ni < 650 µg/g; Co <

468   40 µg/g; Benoit et al., 1996). This observation, together with the absence of clear correlation

469   between Mg# and Ni in whole rock (Fig. 3d), the negative correlation between Mg# and Co in

470   whole rock (Fig. 3e), and with the consistent compositional variations between the different

471   types of dunites, suggests that both pure and impregnated dunites cannot be related by

472   fractional crystallization from a common parent melt. Regarding the pure dunites, a pure

473   cumulative origin does not account for the normalised U-/V-shaped REE patterns (Fig. 5a and

474   5b). The enrichment in LREE relative to MREE is not predicted by REE partition coefficients

475 between olivine and melt (Frey et al., 1978; McKenzie and O'Nions, 1991; Kelemen et al.,

476 1993; Hauri and Hart, 1995; Lee et al., 2007; Sun and Liang, 2014) and may better be explain

477 by melt-rock reactions leading to peridotite metasomatism (e.g. Navon and Stolper, 1987;

478 Godard et al., 1995; Vernières et al., 1997). Models presented in Appendix C evidence that

479 the olivine matrix hosting impregnations exhibit similar REE patterns than for whole rock

480 pure dunites, with the same range of variability. In this way, impregnated dunites may be

481 definitely interpreted as hybrid lithologies, made of a mantle-derived olivine matrix

482 associated to other minerals crystallized during melt percolation (e.g. Rabinowicz et al., 1987;

483 Benn et al., 1988; Boudier and Nicolas, 1995; Koga et al., 2001; Abily and Ceuleneer, 2013;

484 Rospabé et al., 2017). The modelling allows us to conclude that the whole rock trace element

485 signatures of impregnated dunites result from a blend of three main variables: the amount of

486 impregnating mineral phases and their chemical signatures as expected, but also the

487 composition of the dunitic matrix itself (Appendix C).

488

489 *6.3. Melt-rock reaction product: dunitization and melt transport*

490 *6.3.1. State of melt-rock reactions leading to incompatible trace element enrichments in*

491 *mantle peridotites*

492 Incompatible trace element enrichments in peridotites, as U-shaped REE patterns, are

493 documented in numerous peridotites from various tectonic settings, from ophiolitic and

494 orogenic massifs (e.g. Prinzhofer and Allègre, 1985; Bodinier et al., 1990; Gruau et al., 1998;

495 Bouilhol et al., 2009) to abyssal peridotites at mid-ocean ridges (Niu, 2004; Godard et al.,

496 2008) or in forearc context (Parkinson and Pearce, 1998). It has been proposed that melt-rock

497 reactions may lead to some chromatographic effects such as melt-peridotite re-equilibration or

498 to trapped melt between olivine and pyroxene grains. This can be accounted for by (1) a two-

499 stages process involving mantle partial melting later percolated by a LREE-enriched melt (i.e.

500　cryptic metasomatism in the peridotitic matrix without mineralogical reaction) (Navon and

501　Stolper, 1987) or, (2) a single-stage process by combining partial melting (or melt-rock

502　reaction at increasing melt mass; Vernières et al., 1997) and melt transport concomitantly,

503　leading to a MREE depletion relative to HREE whereas LREE remain constant (Godard et al.,

504　1995). In the Oman ophiolite, U-shaped REE patterns were described in mantle harzburgites

505　(Godard et al., 2000; Gerbert-Gaillard, 2002; Girardeau et al., 2002; Le Mée et al., 2004;

506　Monnier et al., 2006; Hanghøj et al., 2010), especially in the Maqsad diapir area where it is

507　attributed to an association between partial melting, deformation related to mantle flow and

508　MORB percolation (Godard et al., 2000; Gerbert-Gaillard, 2002).

509

510　*6.3.2. Extreme trace elements enrichments in DTZ dunites: an early dunitization-related*

511　*signature*

512　The melt-rock reaction leading to dunite formation from a harzburgite through orthopyroxene

513　dissolution is expected to result in a high intergranular permeability of the dunite, that

514　becomes a porous media for efficient melt transfer and extraction (Toramaru and Fujii, 1986;

515　Kelemen et al., 1995b). Dunite channels and horizons, filled or not with troctolitic cumulates,

516　have been mapped within the Maqsad mantle section and interpreted in terms of frozen

517　compaction waves (Ceuleneer et al, 1996; Rabinowicz and Ceuleneer, 2005). They are

518　common features in the Maqsad diapir but not significant in terms of volume. Hence, it is

519　unlikely that the DTZ formed by the transposition in the solid state of such dunitic bodies

520　generated at greater depth, especially since the DTZ dunites do not show any sign of

521　deformation. They better represent the final *in situ* reacting residue of complete dunitization

522　of the uppermost few hundred meters of the mantle induced by melt migration and extraction.

523　Regarding REE, pure dunites from the DTZ display lower HREE, similar and more variable

524　MREE, and higher and more variable LREE contents than harzburgites from the Maqsad

525 mantle section (Fig. 5a) (Godard et al. 2000; Gerbert-Gaillard, 2002). The lower HREE

526 content is in good agreement with a more refractory signature, i.e. depleted, following the

527 complete resorption of orthopyroxene. However, their LREE, Zr, Hf and Th contents are

528 systematically higher than in mantle harzburgites, as Nb, Ta and U in many cases (Fig. 5a and

529 5b). Considering a reacting melt with MORB-like affinities (e.g. Ceuleneer et al., 1996;

530 Benoit et al., 1996; Kelemen et al., 1997a; Abily and Ceuleneer, 2013), these signatures are

531 inconsistent with a genesis at the expense of the surrounding harzburgites alone following the

532 single-stage process described above (Godard et al., 1995; Vernières et al., 1997). Moreover,

533 the occurrence of interstitial minerals implies that the percolating melt suffered crystallization

534 after the harzburgite dunitization, associated to the last stage of percolation during the cooling

535 of the system. Then, one can envision the overprinting of two- or several contemporaneous or

536 successive stages processes in order to explain the dunite trace element signatures. It is worth

537 mentioning that the single- and two-stages processes were proposed in order to mimic

538 harzburgite signatures (Navon and Stolper, 1987; Godard et al., 1995; Vernières et al., 1997),

539 but it may be different for dunites.

540

541 As the trace element enrichment in pure dunites relative to harzburgites cannot be accounted

542 for by V1-type (e.g. Godard et al., 2003) MORB percolation alone, it therefore calls for the

543 additional involvement of a more enriched melt. In the same spirit Godard et al. (2000)

544 proposed the pervasive infiltration of volatile- and LILE-enriched small melt fractions to

545 account for the enrichment in Th, Nb and Ta relative to LREE in mantle harzburgites. The

546 interaction between an incompatible trace elements-enriched melt or fluid and the

547 surrounding dunites does not contradict the percolation of MORB through the DTZ, and the

548 migration of different kinds of melt is further supported by the variable composition of

549 clinopyroxenes located in interstitial position between olivine grains (Fig. 6) (see also Koga et

550   al., 2001) and by the presence of amphibole and orthopyroxene among other which are not

551   expected in the fractionation path of primitive MORB (Rospabé et al., 2017). Furthermore,

552   two strong arguments in favour to MORB percolation through the DTZ are the particularly

553   high CaO content in olivine especially observed in pure dunites (Fig. 4b), consistent with

554   MORB-dunite equilibration before cooling (Abily and Ceuleneer, 2013), and the high TiO_2

555   content in disseminated chromites and impregnant pyroxenes (Fig. 4e and f) (see also

556   Rospabé et al., 2017). In a profile view along the base (pure dunites) of the Buri cross section

557   (Fig. 1b), chemical evolutions from about 640 m to 700 m high show that high CaO values in

558   olivine are strongly correlated to other chemical species (Fig. 8), independently from the very

559   small amount of interstitial clinopyroxene (Table 1). This includes high Gd_{CN}/Yb_{CN} ratio in

560   whole rock (Gd increases from 2.5 to 9.5 ng/g respectively) and a higher concavity of the

561   REE patterns (i.e. well-defined U-/V-shaped REE patterns), but also higher Co content in

562   whole rock and TiO_2 content both in chromite and scarce minute clinopyroxenes. On the

563   contrary, the 700 m level is characterized by lower Fo in olivine (and Ni content both in

564   olivine and whole rock) and La_{CN}/Sm_{CN} ratio in whole rock (faster increase of Sm (from 4.8

565   to 7.8 ng/g) relative to La (from 1.1 to 5.0 ng/g)). Assuming that high CaO in olivine recorded

566   the last re-equilibration with a percolating MORB before cooling (Abily and Ceuleneer,

567   2013), these co-evolutions highlight that dunites had overprinted a prior enrichment in LREE

568   and a strong concave-upward REE pattern signature before the accumulation and the re-

569   equilibration with MORB at 700 m followed by the compaction of the dunitic matrix.

570

571   These observations have several major implications: (1) considering that such enrichments in

572   incompatible elements may be attributable to a low melt-rock ratio (i.e. low porosity) and/or

573   to chromatographic effects induced by the migration of a highly enriched melt (Navon and

574   Stolper, 1987; Godard et al., 1995; Vernières et al., 1997), the low CaO in olivine for the most

575 LREE-enriched samples better supports the re-equilibration with an incompatible elements-

576 rich melt or fluid early in the magmatic history of the DTZ; (2) dunites displaying the highest

577 La_{CN}/Sm_{CN} ratios do not represent an end-member that was percolated by a higher amount of

578 melt (Navon and Stolper, 1987) but result from the more or less significant interaction with

579 this early enriched melt or fluid; (3) the percolation of MORB-type melts did not occur all

580 over the DTZ and seems to have been focused at some particular horizons at an advanced

581 stage of the DTZ structuration (i.e. here the 700 m high level); (4) the increase of the La, Sm

582 and Gd contents until 700 m implies that the re-equilibration with MORB indeed enhanced

583 the enrichment in the most incompatible LREE, but mostly affected and re-enriched the

584 dunitic matrix in the previously most depleted MREE. Especially, from the base to the

585 elevation of 700 m along the Buri cross section, the faster increase of Gd_{CN}/Dy_{CN} (0.33 to

586 0.53) relative to Er_{CN}/Yb_{CN} (0.47 to 0.53) follows the smoothing of MREE-HREE segment

587 pattern. In this way the linear REE patterns in dunites and harzburgites have been interpreted

588 as resulting from re-equilibration induced by MORB-type melt transport (Godard et al.,

589 2000), while concave-upward patterns observed through the DTZ and in mantle harzburgites

590 from the Maqsad area should be better related to the dunitization process. Therefore, MORB

591 percolation led to a decrease of the LREE/MREE and an increase and MREE/HREE ratios,

592 and to smoother REE patterns (i.e. exhibiting a lower concavity). Accordingly, dunites from

593 the DTZ appear to be generated after a multi-stages process: (1) a complete harzburgite

594 reactional melting during which enriched melt batches are generated probably in low volume

595 (i.e. melt generated by the incongruent melting of orthopyroxene associated with the

596 contribution of fluids and minor amount of MORB) followed by (2) a chemical re-

597 equilibration with larger amount of percolating MORB. In opposition with the model of

598 Navon and Stolper (1987), we propose that the incompatible trace elements-enriched

599 signature is a feature acquired early during the dunitization rather than later by the percolation

600   of enriched melts.

601

602   *6.3.3. About the habitus of incompatible trace elements in the dunitic matrix*

603   As previously discussed, the trace element enrichment in dunite, especially in LREE, may

604   better reflect magmatic processes rather than secondary alteration events (paragraph 6.1). It

605   supports the view that trace elements are hosted by the olivine itself rather than by interstitial

606   serpentine surrounding preserved grains and is in accordance with recent trace element data in

607   olivine obtained by laser ablation methods (e.g. Drouin et al., 2009; Rampone et al., 2016;

608   Stead et al., 2017). Sub-solidus re-equilibration between olivine and other mineral phases may

609   eventually occur (Sun and Liang, 2014) and lead to trace element enrichments at olivine

610   grains boundary (Stead et al., 2017), while other studies propose that these particular

611   geochemical signatures reflect analytical artefacts or the entrapment of small LREE-rich melt

612   inclusions (e.g. Lee et al., 2007). The analytical method we developed (Rospabé et al., 2018)

613   allowed us to establish with confidence that the extensive enrichment in LREE relative to

614   MREE in pure dunites (Fig. 5) is a reliable result. These enrichments thus cannot be

615   satisfactorily explained both by analytical effects or re-equilibration with other minerals.

616   Furthermore, we did not detect melt inclusions through microscopic observations and during

617   the electron microprobe sessions, although the existence of inclusions smaller than about 10

618   μm cannot be excluded. Finally, the absence of zoning in olivine grains, at least in terms of

619   major elements, does not militate for a possible concentration of incompatible elements at

620   grain boundaries. All these observations support the hosting of the incompatible trace

621   elements by crystal lattices in olivine consecutively to re-equilibration of the olivine matrix

622   with interstitial melts during their migration through the DTZ. Sub-solidus re-equilibration

623   between different olivine grains may lead to the trace element content smoothing between

624   rims and cores, but stays a hypothetical track at this stage and should be explored in future

625   works.

626

627   *6.4. Refertilization induced by melt transport*

628   Interstitial minerals in impregnated dunites may be considered as crystallization products

629   from a melt percolating through the residual and porous dunitic media (e.g. Benn et al., 1988;

630   Rabinowicz et al., 1987; Kelemen et al., 1995a; Boudier and Nicolas, 1995; Koga et al.,

631   2001), rather than as trapped melts not perfectly extracted (e.g. Faul, 1997; Sundberg et al.,

632   2010). This reasonable assumption is supported by the systematic high Mg# in pyroxenes and

633   generally high An in plagioclases, as well as by the low REE contents both in clinopyroxenes

634   and whole rocks, that are all together not expected in the case of MORB-like melt entrapment

635   between olivine grains (see also Koga et al., 2001). Basically, the whole impregnated dunite

636   composition is strongly impacted by the modal abundance of these interstitial minerals,

637   especially by the amount of clinopyroxene (Fig. 5 and Appendix C).

638

639   *6.4.1. Diversity of the percolating melts within the Maqsad DTZ*

640   Calculated melts in equilibrium with clinopyroxenes impregnating the DTZ appear much

641   more variable than the melts that migrated through the mantle section (Benoit et al., 1996;

642   Benoit, 1997) and the V1 lavas constituting the upper crust in the Sumail massif (Godard et

643   al., 2003) (Fig. 9). Three main types of patterns are observed: clinopyroxenes in equilibrium

644   with (1) a N-MORB type melt (1 sample of cpx-bearing dunite) (Fig. 9a), (2) LREE-enriched

645   melts (mainly in (pl/)cpx-bearing dunites) (Fig. 9b), (3) strongly LREE-depleted melts

646   (mainly in (amph/)opx/pl/cpx-bearing dunites) (Fig. 9c). HREE melt concentrations are

647   basically in the variation range of the MORB-type (or V1, Godard et al., 2003) lavas but are

648   much more variable in LREE. The presence of minerals supposed to be in equilibrium with

649   both LREE-enriched and LREE-depleted melts through the DTZ may reflect either the mixing

650   between various melt batches, including a high proportion of deep melts issued from low

651   mantle partial melting degrees, or the reaction at shallow depth between a primitive MORB

652   and residual depleted peridotites (Sobolev, 1996; Kelemen et al., 1997b; Koga et al., 2001).

653   The first hypothesis would seem unlikely here since the absence of such derived enriched-like

654   cumulates in the mantle section. Indeed, MORB-parent melts that crystallized primitive

655   troctolite sills cropping out in the Maqsad harzburgites show quite geochemical variations

656   attributable to different degrees of partial melting within the diapir (Benoit, 1997), but that are

657   much more restricted than the melt diversity described here.

658

659   *6.4.2. Early generation of enriched melt batches during dunitization*

660   The Maqsad area is characterized by the absence of cumulates crystallized from an enriched

661   parent melt within both the mantle section and the DTZ (Benoit et al., 1996; Kelemen et al.,

662   1997a; Python and Ceuleneer, 2013). According to this and to the trace element enrichments

663   in pure dunites (Fig. 5), we propose the early production of LREE-enriched melts at Moho

664   level (Fig. 9b) further related to melt-rock reactions rather than originated from depth. These

665   melts can be related to the SiO_2-enriched melts produced during incongruent melting of the

666   orthopyroxene and expected following the study of other ophiolitic massifs (Dick, 1977;

667   Quick, 1981; Kelemen, 1990; Kelemen et al., 1992). The early involvement of an enriched

668   melt responsible of the incompatible trace element enrichment in olivine, deduced from the

669   whole pure dunite composition, is in accordance with this interpretation.

670

671   The genesis of highly enriched melts during dunitization, and the incipient crystallization,

672   may be related to reactive crystallization (Collier and Kelemen, 2010). This process was

673   identified as the main cause of clinopyroxene chemical zoning in olivine-rich troctolites from

674   slow spreading environments: cores were generated by fractional crystallization from a

675 percolating melt while enriched rims result from the fractionation after the contamination of

676 the melt by assimilation of the surrounding peridotite (e.g. Suhr et al., 2008; Drouin et al.,

677 2009; Sanfilippo et al., 2013, 2015; Rampone et al., 2016). Especially, the resorption of

678 orthopyroxene seems to be a credible source for this particular signature, allowing to

679 important Zr_{CN}/Nd_{CN} fractionation (until 1.5) with the increase of REE contents (Sanfilippo et

680 al., 2015). In this way, the dunitization, when directly followed by interstitial mineral

681 fractionation, can be presented as a kind of reactive crystallization process considering the

682 enrichment in silica and incompatible trace elements of the residual melt. However, in this

683 study, clinopyroxene grains analyzed for their trace elements are not zoned and present low

684 Zr_{CN}/Nd_{CN} ratios (0.34-0.74; 0.47 in average) with no observed correlation with Yb, similar to

685 clinopyroxene cores in olivine-rich troctolites. This highlights that the chemical evolution of

686 enriched melt batches is probably, in the frame of the Maqsad DTZ, firstly dominated by the

687 residual orthopyroxene assimilation process by MORB (i.e. reactive crystallization in the case

688 of clinopyroxene fractionation at this stage). Following the complete orthopyroxene

689 resorption, fractional crystallization occurs while MORB issued from partial melting within

690 the Maqsad diapir are introduced and transferred through the porous olivine matrix without

691 any further reaction.

692

693 *6.4.3. Differentiation and hybridization of the percolating melts within the Maqsad DTZ*

694 Oppositely, further hypotheses may be proposed concerning the LREE-depleted melts (Fig.

695 9c), which may reflect (1) the assimilation of the surrounding dunite at an advanced

696 refertilization stage (i.e. reactive crystallization products), (2) the later sub-solidus re-

697 equilibration between clinopyroxene crystals and neighbouring mineral phases (e.g. Sun and

698 Liang, 2014), (3) the result of hybridization between a latter percolating MORB and hydrous

699 fluids (Rospabé et al. 2017). The two first hypotheses difficultly account for the large

700 chemical variations in clinopyroxene, that is the most common and abundant impregnant

701 phase in DTZ dunites, especially concerning the variable slope of the HREE segment (Figs. 6

702 and 9). However, the third hypothesis is supported by the fact that the LREE-depleted

703 signature is observed mainly in samples containing interstitial orthopyroxene and/or

704 amphibole, minerals previously interpreted as fractionated from a hybrid melt between

705 MORB and hydrous fluids (Rospabé et al., 2017). In this scenario this hybrid component may

706 contribute to the exotic melt involved in the formation of disseminated chromites and

707 chromitite ore bodies as suggested by the numerous inclusions of hydrous minerals in

708 chromite (Lorand et Ceuleneer, 1989; Leblanc et Ceuleneer, 1991; Borisova et al., 2012;

709 Rospabé et al., 2017; Johan et al., 2017).

710

711 To conclude, our study reveals that the variability in the composition of the melts responsible

712 of the dunite formation and of their petrological and geochemical evolution is extremely

713 pronounced (see also Sanfilippo et al., 2014, 2017). A working hypothesis is to consider that

714 such wide melt variability is a specificity of the DTZ and reflects local melt/fluid-rock

715 reactions rather than a complex mixing of deep-seated melt batches. This assumption is

716 supported by the fact that some clinopyroxene grains exhibiting different patterns were

717 analysed in samples collected in nearly same locations (Table 1 and Appendix B). According

718 to the observed clinopyroxene chemical heterogeneity, it appears that the DTZ evolved as an

719 open reactive system in which melts fractions issued from strong melt-rock interactions

720 evolved by fractional crystallization and hybridization and were far from being fully

721 homogenised before being supplied to the lower crust.

722

723 *6.5. Synthetic model for the formation of the Maqsad DTZ*

724 As pointed out here above, none of the four main processes that are discussed - (1)

725 serpentinization or secondary weathering, (2) fractionation and accumulation of olivine, (3)

726 harzburgite reactional melting and re-equilibration related to melt percolation into dunite

727 porosity, and (4) refertilization through minerals crystallization from percolating melts

728 interstitially between olivine grains - may account alone for the wide spectrum of

729 geochemical signatures observed in whole rock and mineral compositions of the DTZ,

730 although each can contribute to account for part of this variability, depending on the elements

731 considered. This indicates that the DTZ records an overprinting of several processes.

732

733 In attempt to propose a general scenario describing the development of the Maqsad DTZ,

734 Figure 10 summarizes the different steps deduced from the whole rock and mineral major and

735 trace element signatures. The starting lithology, i.e. the harzburgite from the specific Maqsad

736 area, present a slight but significant LREE enrichment relative to the harzburgites from the

737 main mantle section located far away from the diapir (Fig. 10a) (Godard et al., 2000). Acting

738 as a filter for ascending melts, the top of the diapir is progressively transformed into dunites

739 by interaction with interstitial melts, probably of MORB affinity (Fig. 10b). This process

740 leads to the depletion in HREE in the residual dunite due to the resorption of the last

741 pyroxenes and to the enrichment in LREE and other incompatible trace elements (HFSE, Th,

742 U and possibly some LILE as Rb and Ba). This signature is better explained by the early

743 generation of small batches of enriched melts in response to orthopyroxene incongruent

744 melting (i.e. enriched residual melt). At start, the reaction is driven by MORB/harzburgite

745 interaction but the olivine matrix records the solely incompatible trace elements enrichment,

746 calling for a very low porosity needed to preserve this signature. It has been proposed that

747 high temperature hydrothermal fluids were involved in dunite formation or as early as the

748 mantle dunitization process (Bowen and Tuttle, 1949; Rospabé et al., 2017; Johan et al.,

749 2017); the enriched signature described in this paper may be another evidence for the early

750   hydration of the DTZ. Following this, the dunitization will increase the permeability, as

751   MORB-like melts delivered by the mantle continue to invade the matrix. Those melts no

752   longer contribute to mineralogical reaction following the complete orthopyroxene resorption

753   within the host rock, and then may accumulate at Moho level or feed the crust (Fig. 10c and

754   10d). Chemical re-equilibration occurs during MORB percolation, leading to a slight LREE

755   and mainly MREE enrichment in the host dunite, i.e. the re-equilibration process seems to

756   mainly affect the most depleted trace elements in the dunitic matrix independently from the

757   partition coefficient between those elements and olivine. The chemical overprinting of this

758   stage occurs until the compaction of the matrix and the resulting melt extraction. It is worth

759   mentioning that all the intermediate cases may exist between a pure dunite having preserved

760   its prior enriched signature (Fig. 10e) and another one having been fully re-equilibrated with

761   MORB (Fig. 10f). Therefore, pure dunites may be considered as a witness of a magmatic

762   system closed at very high temperature (i.e. above the olivine-plagioclase-clinopyroxene

763   ternary cotectic). Depending on the thermal state of the DTZ, and certainly on the primitive or

764   evolved nature of the percolating melt, crystallization will or not occur interstitially. As

765   supposed following the various REE patterns calculated for the olivine matrix hosting some

766   impregnating clinopyroxene (Appendix C), mineral fractionation occurs concomitantly with

767   the melt percolation and re-equilibration processes (Fig. 10g). Among other, the circulation of

768   hydrous fluids at Moho level during the structuration of the DTZ explains: (1) the higher

769   amount of impregnations approaching the base of the crust witnessing the former thermal

770   gradient across DTZ (Rospabé et al., 2017; see also Dygert et al., 2017), (2) the harzburgite

771   dunitization in the specific context of the DTZ, and not to deeper dunite channels within the

772   mantle section, and (3) the interstitial mineralogy indicative of the percolation of exotic

773   hybrid melts certainly involved in the transport of high amount of Cr - potentially released

774   from orthopyroxene during the dunitization (Johan et al., 2017) - and its concentration in

775 disseminated chromites and chromitite pods (Rospabé et al., 2017). In the case of a much

776 colder environment as in slower-spreading environment (Collier and Kelemen, 2010),

777 extreme refertilization potentially occur through a more efficient assimilation of the olivine

778 matrix coupled to fractional crystallization (reactive crystallization), leading to the formation

779 of olivine-rich troctolites as observed in samples collected along present-day mid-ocean

780 ridges or within ophiolites DTZ (e.g. Suhr et al., 2008; Drouin et al., 2009; Dick et al., 2010;

781 Sanfilippo and Tribuzio, 2013b; Sanfilippo et al., 2013, 2014, 2015; Rampone et al., 2016).

782 At this stage, it cannot be excluded that the fractional crystallization dominated the

783 refertilization process within the Maqsad DTZ, relative to reactive crystallization, due to the

784 fast spreading environment in which the Oman ophiolite likely evolved. Another possibility

785 consists in the fast cooling of this oceanic lithosphere fragment, related to the oceanic

786 thrusting that directly followed the lithosphere accretion and that fossilized the system in a

787 high temperature configuration (Boudier et al., 1988). Finally, in regard to the whole dunites

788 and mineral major and trace elements, it appears that both pure and variably impregnated

789 dunites represent end-members that can be generated independently.

790

791 As shown, the re-equilibration with percolating MORB did not occur equally all along the

792 DTZ but was more efficient at some specific levels (Fig. 8) (see also Abily and Ceuleneer,

793 2013), suggesting that the dunitic matrix was either unequally compacted when MORB

794 migrated through it or that the MORB percolation was locally focused. This feature may be

795 partially explained by a model of progressive downward dunitization of the mantle

796 harzburgites at the top of the Maqsad diapir (Abily and Ceuleneer, 2013). During this process,

797 the compaction may progress downward, possibly in response from cooling from above,

798 through successive steps and then may spatially constrain the porous fronts in which MORB

799 may have accumulated. Clearly, some horizons of the DTZ remained isolated early after

800   dunitization and other horizons were intensely re-equilibrated with MORB more or less

801   hybridized with hydrous, likely hydrothermal fluids.

802

803   **7. Conclusion**

804   Major and trace elements of 79 pure to highly impregnated dunites from the Oman ophiolite

805   and the composition of the impregnation minerals revealed a large petrological and chemical

806   variability. The dunitic matrix - measured pure dunites and modelled olivine matrix in

807   impregnated dunites - is characterized by a more or less pronounced concave-upward REE

808   pattern and a variable enrichment in other incompatible HFSE, Th, U, Rb and Ba. Their REE

809   and multi-elements patterns are highly scattered implying that no dominant single process

810   controlled the dunite formation. Chemical evolutions suggest that the enriched signature was

811   recorded early during the dunitization by interaction between the surrounding olivine matrix

812   and incompatible trace elements-rich small melt batches at low melt/rock ratios. The latest

813   MORB percolation leads to a cryptic metasomatism expressed as smoothest REE patterns,

814   among others, inducing flattest slopes in HREE and LREE patterns. This scenario contradicts

815   the later percolation of a deep-seated enriched melt and better supports that hybrid enriched

816   melts are generated by melt/rock reactions at an early magmatic stage within the DTZ beneath

817   mid-ocean spreading centers.

818

819   Our survey shows that these different signatures are variably distributed along the DTZ. This

820   implies that some horizons have been compacted early immediately following the mantle

821   harzburgites dunitization, while others maintained a high enough permeability to drain

822   MORB and make possible re-equilibration. The physical processes that condition the

823   heterogeneous chemical distribution along the DTZ remains quite enigmatic at this stage.

824   Pure and impregnated dunites may be considered as two lithological end-members starting

825 from a common dunitized peridotitic matrix: the first have been compacted at very high

826 temperature after various chemical re-equilibration degrees and the complete extraction of

827 interstitial percolating melts, while the others have been modally refertilized before the

828 extraction of the residual melt. In this frame, the combination of whole dunites and *in situ*

829 minerals major and trace elements compositions reveals undoubtedly the multi-stages

830 processes involved in the DTZ generation.

831

832 Finally, based on the chemical variability within the different minerals observed in dunites

833 from the DTZ, we conclude that if MORB magmas generated by mantle partial melting may

834 have been partly homogenized within the uppermost mantle before being supplied to the

835 mantle-crust transition zone, melt-rock reactions and hybridization processes occurring within

836 the DTZ may generate new, exotic and/or hybrid, melt batches that will participate to the

837 oceanic crust genesis and potentially to the MORB heterogeneity. The precise relationship

838 between the evolution of the Maqsad diapir, the N130 paleo-ridge axis, and the vertical

839 petrological and geochemical signatures across the DTZ is a complex three-dimensional

840 problem and could be deciphered by a more comprehensive structural, petrological and

841 geochemical survey of the area.

842

857

858 **Figure 1.** Geological map of the Oman ophiolite showing (1) the spatial distribution of the

859 mantle and crustal sections and (2) the two main magmatic suites displayed along the

860 ophiolite regarding the nature of the dikes cross-cutting the mantle section, characterized as

861 the depleted-andesitic series and the and N-MORB tholeiitic one (a). The Sumail massif

862 exposes a dunitic transition zone of about 300 m thick above the Maqsad mantle diapir (b).

863 Four cross sections were sampled in this area.

864

865 **Figure 2.** Photomicrographs illustrating the mineralogical diversity that allowed to define the

866 different lithological facies observed within the Oman ophiolite DTZ, with the olivines

867 constituting the matrix of a pure dunite (a), the comparison between a well developed

868 impregnant clinopyroxene oikocryst in a cpx-bearing dunite (b) with a small interstitial

869 diopside in a pure dunite (c), a plagioclase oïkocryst in a pl/cpx-bearing dunite (d), an

870 orthopyroxene oikocryst in a opx/pl/cpx-bearing dunite (e), and an amphibole in a amphibole-

871 bearing dunite.

872

873 **Figure 3.** Whole rock major and minor element compositions of the studied dunites in the

874 Maqsad dunites (coloured circles) compared to other DTZ dunites (open circles), mantle

875   harzburgites (open squares) and cpx-harzburgites/lherzolites (open diamonds) from the Oman

876   ophiolite (Godard et al., 2000; Gerbert-Gaillard, 2002; Takazawa et al., 2003; Monnier et al.,

877   2006; Hanghøj et al., 2010; Khedr et al., 2014; Nicolle et al., 2016). (a) MgO/SiO_2 versus

878   Al_2O_3/SiO_2, (b) total iron as FeO versus MgO, (c) Al_2O_3 versus CaO, and (d) Ni and (e) Co as

879   a function of the Mg# ratio ($100 \times$ molar $Mg/(Mg + Fe_{total})$). Compositions are recalculated on

880   a volatile-free basis. Grey bar in panel (a) represents the silicate Earth differentiation trend (or

881   "terrestrial array") (Jagoutz et al., 1979). Dashed black line in panel (b) represents the

882   variation of olivine composition constrained by FeO + MgO = 66.67 mol% following Godard

883   et al. (2000). Dashed grey lines in panels (b) and (c) represent constant Mg# and Al_2O_3/CaO

884   ratios respectively.

885

886   **Figure 4.** Mineral major element compositions of the studied dunites from the Maqsad area

887   illustrated in (a) NiO in olivine, (b) CaO in olivine and (c) Mg# in whole rock as a function of

888   Fo in olivine, in (d) Cr# ($100 \times$ molar $Cr/(Cr + Al)$ in chromite versus Fo in olivine with the

889   olivine-spinel mantle array (OSMA) from (Arai, 1987; Arai, 1994) (grey field), (e) TiO_2

890   versus Mg# ratio ($100 \times$ molar $Mg/(Mg + Fe^{2+})$ in chromite and (f) TiO_2 as a function of Mg#

891   ratio ($100 \times$ molar $Mg/(Mg + Fe^{2+})$ in clinopyroxene. Dark blue dots in clinopyroxene plots

892   are the small diopsides observed at olivine grains rims in both pure and impregnated dunites.

893   They are plotted whatever their hosting lithological facies, displaying a composition range

894   spanning between igneous clinopyroxenes and pure hydrothermal diopsides (Rospabé et al.,

895   2017).

896

897   **Figure 5.** Whole rock chondrite-normalized REE (a, c, e and g) and Primitive Mantle-

898   normalized multi-elements (b, b, f and h) patterns of the studied dunites from the Maqsad

899   dunitic transition zone. Colour labels following the figure 2 for pure dunites (a and b), cpx-

900 bearing dunites (c and d), pl/cpx-bearing dunites (e and f), and opx/pl/cpx-bearing dunites and

901 amphibole-bearing dunites (±opx, pl and cpx) (g and h). In the panels (a) and (b) pure dunites

902 patterns (blue lines) are compared to the harzburgites from the whole Oman ophiolite mantle

903 section (white field framed with a dashed black line) (Gerbert-Gaillard, 2002; Takazawa et

904 al., 2003; Monnier et al., 2006; Hanghøj et al., 2010; Khedr et al., 2014; Nicolle et al., 2016)

905 and to the main mantle harzburgites from the Sumail massif (light grey field), the harzburgites

906 from the Maqsad diapir area (medium grey field) and few other dunites from the Maqsad

907 DTZ (dark grey field) (Godard et al., 2000; Gerbert-Gaillard, 2002). In other panels each

908 lithological facies is compared to the field of pure dunites from this study (blue fields).

909 Normalizing chondrite and Primitive Mantle values are from Barrat et al. (2012) and Sun and

910 McDonough (1989) respectively.

911

912 **Figure 6.** Clinopyroxene chondrite-normalized REE (a) and Primitive Mantle-normalized

913 multi-elements patterns (b). Normalizing chondrite and Primitive Mantle values are from

914 Barrat et al. (2012) and Sun and McDonough (1989) respectively.

915

916 **Figure 7.** Trace element co-evolutions in pure dunites represented as (a) La, (b) U, (c) Zr, (d)

917 Ta, (e) Rb and (f) Ba as a function of Th.

918

919 **Figure 8.** Chemical evolutions along the base of the Buri cross section, made of pure dunites,

920 illustrated in Fo and NiO in olivine, and whole rock La_{CN}/Sm_{CN} and Gd_{CN}/Yb_{CN} ratios as well

921 as the degree of concavity of their REE patterns, all as a function of the absolute elevation of

922 the sampling site. The concavity of the REE patterns was calculated for each sample as

923 $[\sqrt{(Sm_{CN} \times Gd_{CN})}/\sqrt{(Ce_{CN} \times Yb_{CN})} -1]$. All these co-evolutions are a further strong evidence

924 for the hosting of incompatible trace elements by olivine itself.

925

Figure 9. Calculated equilibrium melts with the interstitial clinopyroxenes in impregnated dunites from the Maqsad DTZ. Clinopyroxene compositions were averaged for each sample to perform the calculation. Compositions are presented following the shape of the REE patterns with (a) MORB-type melts, (b) LREE-enriched melts and (c) LREE-depleted melts. Calculated melts are compared to the Oman ophiolite V1 (red field) and V2 (green fields) lavas (Godard et al., 2003; Godard et al., 2006) and boninites (dark green field) (Ishikawa et al., 2002; Ishikawa et al., 2005). N-MORB values are from Sun and McDonough (1989). Partitioning coefficients used in the calculation are from Bédard (1994) and normalizing chondrite values are from Barrat et al. (2012). It is worth mentioning that clinopyroxene is the most abundant impregnating phase, and is supposed to display the higher trace element contents in dunites, together with amphibole. In regard of the large HREE content variations in clinopyroxene, it is difficult to account for this variability following sub-solidus re-equilibration with other minerals present (e.g. Sun and Liang, 2014), especially in the restricted temperature range expected with the cotectique ol-pl-cpx. Thus it is assumed that re-equilibration between clinopyroxene and neighbouring olivine, orthopyroxene, plagioclase and/or amphibole is negligible as far as the REE are concerned (i.e. the assumption of a low REE diffusivity at subsolidus temperature following Van Orman et al., 2001). Then, the calculation of the inferred melt in equilibrium from which the clinopyroxene crystallized allows investigating the nature of the melt that percolated and fractionated interstitial minerals through dunitic rocks.

Figure 10. Synthetic model for the genesis of the dunites from the Maqsad DTZ, summarizing the melt-rock reactions leading to their high petrological and geochemical variability: (a) incongruent melting of orthopyroxene in mantle harzburgites just below Moho

level, (b) neo-formed dunite comprising interstitial high-silica and trace elements-enriched small melt batches, (c) MORB infiltration within the porosity, leading to a hybridization process between the former enriched melt and the incoming MORB, and (d) intense migration of variably evolved MORB batches, leading to variably extensive chemical re-equilibration with the surrounding dunitic matrix. Pure dunites may be produced at different stages over the successive melt-rock reactions, directly following the dunites genesis when they are enriched in the most incompatible elements as LREE (U-shaped REE pattern as the blue line) (e), or after strong re-equilibration with the percolating MORB that allowed to the enrichment in MREE in the olivine matrix (i.e. smoothing of the REE pattern) (f). The chemical signature of pure dunites will first depend on the amount of melt that percolated and re-equilibrated with the host dunites and second on the chemistry of this melt. In some cases, mineral crystallization occurs through the DTZ leading to the formation of impregnated dunites after extraction of the residual melt and compaction of the matrix (g). Refertilization may occur at any moment of the evolution of the system, either within a neo-formed dunite or within a fully re-equilibrated one after intense MORB percolation. In that case the whole rock chemical signature will depend on (1) the composition of the olivine matrix, (2) the amount of fractionated minerals interstitially and (3) the composition of these minerals.

Table 1. Location and modal composition of the samples analysed in this study. The modal abundance of each mineral was calculated using both whole rock and mineral major elements. Mode calculations were systematically compared to and are in good agreement with thin section observations.

Appendix A. Whole rock major and trace element compositions.

975   **Appendix B.** Mineral major element compositions and clinopyroxene trace element

976   compositions.

977

978   **Appendix C.** Modelling of the interstitial minerals modal abundance influence on the whole

979   rock chemical content

980

981   **References**

982   Abily B. and Ceuleneer G. (2013) The dunitic mantle-crust transition zone in the Oman

983   ophiolite: Residue of melt-rock interaction, cumulates from high-MgO melts, or both?

984   *Geology* **41**, 67-70.

985   Akizawa N., Ozawa K., Tamura A., Michibayashi K. and Arai S. (2016a) Three-dimensional

986   evolution of melting, heat and melt transfer in ascending mantle beneath a fast-spreading

987   ridge segment constrained by trace elements in clinopyroxene from concordant dunites

988   and host harzburgites of the Oman ophiolite. *J. Petrol.* **57**, 777-814.

989   Akizawa N., Tamura A., Fukushi K., Yamamoto J., Mizukami T., Python M. and Arai S.

990   (2016b) High-temperature hydrothermal activities around suboceanic Moho: An example

991   from diopsidite and anorthosite in Wadi Fizh, Oman ophiolite. *Lithos* **263**, 66-87.

992   Arai S. (1987) An estimation of the least depleted spinel peridotite on the basis of olivine-

993   spinel mantle array. *Neues Jahrb. für Mineral. - Monatshefte* **8**, 347-354.

994   Arai S. (1994) Characterization of spinel peridotites by olivine-spinel compositional

995   relationships: Review and interpretation. *Chem. Geol.* **113**, 191-204.

996   Arai S. and Matsukage K. (1996) Petrology of gabbro-troctolite-peridotite complex from Hess

997   Deep, equatorial Pacific: implications for mantle-melt interaction within the oceanic

998   lithosphere. *Proc. Ocean Drill. Program, Sci. Results* **147**, 135-155.

999   Bach W., Garrido C. J., Paulick H., Harvey J. and Rosner M. (2004) Seawater-peridotite

1000   interactions: First insights from ODP Leg 209, MAR 15°N. *Geochemistry, Geophys.*

1001   *Geosystems* **5**.

1002   Barrat J.-A., Keller F., Amossé J., Taylor R. n., Nesbitt R. w. and Hirata T. (1996)

1003   Determination of Rare Earth Elements in Sixteen Silicate Reference Samples by Icp-Ms

1004   After Tm Addition and Ion Exchange Separation. *Geostand. Newsl.* **20**, 133-139.

1005   Barrat J.-A., Zanda B., Moynier F., Bollinger C., Liorzou C. and Bayon G. (2012)

1006   Geochemistry of CI chondrites: Major and trace elements, and Cu and Zn Isotopes.

1007   *Geochim. Cosmochim. Acta* **83**, 79-92.

1008   Bédard J. H. (1994) A procedure for calculating the equilibrium distribution of trace elements

1009   among the minerals of cumulate rocks, and the concentration of trace elements in the

1010   coexisting liquids. *Chem. Geol.* **118**, 143-153.

1011   Bédard J. H. and Hébert R. (1998) Formation of chromitites by assimilation of crustal

1012   pyroxenites and gabbros into peridotitic intrusions: North Arm Mountain massif, Bay of

1013   Islands ophiolite, Newfoundland, Canada. *J. Geophys. Res. Earth* **103**, 5165-5184.

1014   Benn K., Nicolas A. and Reuber I. (1988) Mantle-crust transition zone and origin of wehrlitic

1015   magmas: Evidence from the Oman ophiolite. *Tectonophysics* **151**, 75-85.

1016   Benoit M. (1997) Caractérisation géochimique (traces, isotopes) d'un système de drainage

1017   magmatique fossile dans l'ophiolite d'Oman. *PhD thesis* Université Toulouse III - Paul

1018   Sabatier, 257 pp.

1019   Benoit M., Ceuleneer G. and Polvé M. (1999) The remelting of hydrothermally altered

1020   peridotite at mid-ocean ridges by intruding mantle diapirs. *Nature* **402**, 514-518.

1021   Benoit M., Polvé M. and Ceuleneer G. (1996) Trace element and isotopic characterization of

1022   mafic cumulates in a fossil mantle diapir (Oman ophiolite). *Chem. Geol.* **134**, 199-214.

1023   Berger E. T. and Vannier M. (1984) Les dunites en enclaves dans les basaltes alcalins des iles

1024   oceaniques: approche petrologique. *Bull. Mineral.* **107**, 649-663.

1025 Bodinier J. L., Vasseur G., Vernières J., Dupuy C. and Fabries J. (1990) Mechanisms of

1026   Mantle Metasomatism: Geochemical Evidence from the Lherz Orogenic Peridotite. *J.*

1027   *Petrol.* **31**, 597-628.

1028 Borisova A. Y., Ceuleneer G., Kamenetsky V. S., Arai S., Béjina F., Abily B., Bindeman I.

1029   N., Polvé M., De parseval P., Aigouy T. and Pokrovski G. S. (2012) A new view on the

1030   petrogenesis of the Oman ophiolite chromitites from microanalyses of chromite-hosted

1031   inclusions. *J. Petrol.* **53**, 2411-2440.

1032 Boschi C., Dini A., Früh-Green G. L. and Kelley D. S. (2008) Isotopic and element exchange

1033   during serpentinization and metasomatism at the Atlantis Massif (MAR 30°N): Insights

1034   from B and Sr isotope data. *Geochim. Cosmochim. Acta* **72**, 1801-1823.

1035 Boudier F., Bouchez J. L., Nicolas A., Cannat M., Ceuleneer G., Misseri M. and Montigny R.

1036   (1985) Kinematics of oceanic thrusting in the Oman ophiolite: model of plate

1037   convergence. *Earth Planet. Sci. Lett.* **75**, 215-222.

1038 Boudier F., Ceuleneer G. and Nicolas A. (1988) Shear zones, thrusts and related magmatism

1039   in the Oman ophiolite: Initiation of thrusting on an oceanic ridge. *Tectonophysics* **151**,

1040   275-296.

1041 Boudier F. and Coleman R. G. (1981) Cross section through the peridotite in the Samail

1042   Ophiolite, southeastern Oman Mountains. *J. Geophys. Res. Solid Earth* **86**, 2573-2592.

1043 Boudier F. and Nicolas A. (1995) Nature of the moho transition zone in the Oman ophiolite.

1044   *J. Petrol.* **36**, 777-796.

1045 Bouilhol P., Burg J. P., Bodinier J. L., Schmidt M. W., Dawood H. and Hussain S. (2009)

1046   Magma and fluid percolation in arc to forearc mantle: Evidence from Sapat (Kohistan,

1047   Northern Pakistan). *Lithos* **107**, 17-37.

1048 Bowen N. L. (1915) The later stages of the evolution of the igneous rocks. *J. Geol.* **23**, 1–91.

1049 Bowen N. L. (1927) The Origin of ultra-basic and related rocks. *Am. J. Sci.* **14**, 89-108.

1050   Bowen N. L. and Tuttle O. F. (1949) The System MgO-SiO$_2$-H$_2$O. *Geol. Soc. Am. Bull.* **60**,

1051   439.

1052   Ceuleneer G. (1986) Structure des ophiolites d'Oman : flux mantellaire sous un centre

1053   d'expansion océanique et charriage à la dorsale. *PhD thesis* Université de Nantes, 349

1054   pp.

1055   Ceuleneer G. (1991) Evidence for a Paleo-Spreading Center in the Oman Ophiolite: Mantle

1056   Structures in the Maqsad Area. In Springer Netherlands. pp. 147-173.

1057   Ceuleneer G. and le Sueur E. (2008) The Trinity ophiolite (California): The strange

1058   association of fertile. *Bull. la Soc. Geol. Fr.* **179**, 503-518.

1059   Ceuleneer G., Monnereau M. and Amri I. (1996) Thermal structure of a fossil mantle diapir

1060   inferred from the distribution of mafic cumulates. *Nature* **379**, 149-153.

1061   Ceuleneer G., Nicolas A. and Boudier F. (1988) Mantle flow pattern at an oceanic spreading

1062   centre: the Oman peridotite record. *Tectonophysics* **151**, 1-26.

1063   Clénet H., Ceuleneer G., Pinet P., Abily B., Daydou Y., Harris E., Amri I. and Dantas C.

1064   (2010) Thick sections of layered ultramafic cumulates in the Oman ophiolite revealed by

1065   an airborne hyperspectral survey: Petrogenesis and relationship to mantle diapirism.

1066   *Lithos* **114**, 265-281.

1067   Coleman R. G. and Keith T. E. (1971) A chemical study of serpentinization-burro mountain,

1068   California. *J. Petrol.* **12**, 311-328.

1069   Collier M. L. and Kelemen P. B. (2010) The case for reactive crystallization at mid-ocean

1070   ridges. *J. Petrol.* **51**, 1913-1940.

1071   Daines M. J. and Kohlstedt D. L. (1994) The transition from porous to channelized flow due

1072   to melt/rock reaction during melt migration. *Geophys. Res. Lett.* **21**, 145-148.

1073   Deschamps F., Godard M., Guillot S. and Hattori K. (2013) Geochemistry of subduction zone

1074   serpentinites: A review. *Lithos* **178**, 96-127.

1075   Dick H. J. B. (1977) Evidence of partial melting in the Josephine peridotite. *Magma Genes.*
1076   **96**, 59-62.

1077   Dick H. J. B., Johan Lissenberg C. and Warren J. M. (2010) Mantle melting, melt transport,
1078   and delivery beneath a slow-spreading ridge: The paleo-MAR from 23°15'N to 23°45'N.
1079   *J. Petrol.* **51**, 425-467.

1080   Dick H. J. B. and Natland J. H. (1996) Late-stage melt evolution and transport in the shallow
1081   mantle beneath the East Pacific Rise. *Proc. ODP Sci. Res.* **147**, 103-134.

1082   Drouin M., Godard M., Ildefonse B., Bruguier O. and Garrido C. J. (2009) Geochemical and
1083   petrographic evidence for magmatic impregnation in the oceanic lithosphere at Atlantis
1084   Massif, Mid-Atlantic Ridge (IODP Hole U1309D, 30°N). *Chem. Geol.* **264**, 71-88.

1085   Dygert N., Kelemen P. B. and Liang, Y. (2017) Spatial variations in cooling rate in the mantle
1086   section of the Samail ophiolite in Oman: Implications for formation of lithosphere at
1087   mid-ocean ridges. *Earth Planet. Sci. Lett.* **465**, 134-144.

1088   Elthon D. (1979) High magnesia liquids as the parental magma for ocean floor basalts. *Nature*
1089   **278**, 514-518.

1090   Faul U. H. (1997) Permeability of partially molten upper mantle rocks from experiments and
1091   percolation theory. *J. Geophys. Res.* **102**, 10299.

1092   Frey F. A., Green D. H. and Roy S. D. (1978) Integrated models of basalt petrogenesis: A
1093   study of quartz tholeiites to olivine melilitites from South Eastern Australia utilizing
1094   geochemical and experimental petrological data. *J. Petrol.* **19**, 463-513.

1095   Gerbert-Gaillard L. (2002) Caractérisation Géochimique des Péridotites de l'ophiolite
1096   d'Oman : Processus Magmatiques aux Limites Lithosphère/Asthénosphère. *PhD Thesis*
1097   Université Montpellier II - Sciences et Techniques du Languedoc, 238 pp.

1098   Ghosh B., Morishita T., Gupta B. Sen, Tamura A., Arai S. and Bandyopadhyay D. (2014)
1099   Moho transition zone in the Cretaceous Andaman ophiolite, India: A passage from the

1100 mantle to the crust. *Lithos* **198–199**, 117-128.

1101 Girardeau J., Monnier C., Le Mée L. and Quatrevaux F. (2002) The Wuqbah peridotite,

1102 central Oman Ophiolite: Petrological characteristics of the mantle in a fossil overlapping

1103 ridge setting. *Mar. Geophys. Res.* **23**, 43-56.

1104 Godard M., Bodinier J. and Vasseur G. (1995) Effects of mineralogical reactions on trace

1105 element redistributions in mantle rocks during percolation processes : A chromatographic

1106 approach. *Earth Planet. Sci. Lett.* **133**, 449-461.

1107 Godard M., Bosch D. and Einaudi F. (2006) A MORB source for low-Ti magmatism in the

1108 Semail ophiolite. *Chem. Geol.* **234**, 58-78.

1109 Godard M., Dautria J. M. and Perrin M. (2003) Geochemical variability of the Oman

1110 ophiolite lavas: Relationship with spatial distribution and paleomagnetic directions.

1111 *Geochemistry, Geophys. Geosystems* **4**.

1112 Godard M., Jousselin D. and Bodinier J. L. (2000) Relationships between geochemistry and

1113 structure beneath a palaeo-spreading centre: A study of the mantle section in the Oman

1114 ophiolite. *Earth Planet. Sci. Lett.* **180**, 133-148.

1115 Godard M., Lagabrielle Y., Alard O. and Harvey J. (2008) Geochemistry of the highly

1116 depleted peridotites drilled at ODP Sites 1272 and 1274 (Fifteen-Twenty Fracture Zone,

1117 Mid-Atlantic Ridge): Implications for mantle dynamics beneath a slow spreading ridge.

1118 *Earth Planet. Sci. Lett.* **267**, 410-425.

1119 Green D. H. and Ringwood A. E. (1967) The genesis of basaltic magmas. *Contrib. to*

1120 *Mineral. Petrol.* **15**, 103-190.

1121 Gruau G., Bernard-Griffiths J. and Lécuyer C. (1998) The origin of U-shaped rare earth

1122 patterns in ophiolite peridotites: assessing the role of secondary alteration and melt/rock

1123 reaction. *Geochim. Cosmochim. Acta* **62**, 3545-3560.

1124 Hanghøj K., Kelemen P. B., Hassler D. and Godard M. (2010) Composition and genesis of

1125   depleted mantle peridotites from the Wadi Tayin massif, Oman ophiolite; Major and

1126   trace element geochemistry, and Os isotope and PGE systematics. *J. Petrol.* **51**, 201-227.

1127 Hauri E. H. and Hart S. R. (1995) Correction to "Constraints on melt migration from mantle

1128   plumes: A trace element study of peridotite xenoliths from Savai'i, Western Samoa" by

1129   Erik H. Hauri and Stanley R. Hart. *J. Geophys. Res. Solid Earth* **100**, 2003-2003.

1130 Herzberg C. T., Fyfe W. S. and Carr M. J. (1983) Density constraints on the formation of the

1131   continental Moho and crust. *Contrib. to Mineral. Petrol.* **84**, 1-5.

1132 Ishikawa T., Fujisawa S., Nagaishi K. and Masuda T. (2005) Trace element characteristics of

1133   the fluid liberated from amphibolite-facies slab: Inference from the metamorphic sole

1134   beneath the Oman ophiolite and implication for boninite genesis. *Earth Planet. Sci. Lett.*

1135   **240**, 355-377.

1136 Ishikawa T., Nagaishi K. and Umino S. (2002) Boninitic volcanism in the Oman ophiolite:

1137   Implications for thermal condition during transition from spreading ridge to arc. *Geology*

1138   **30**, 899-902.

1139 Jagoutz E., Palme H., Baddenhausen H., Blum K., Cendales M., Dreibus G., Spettel B.,

1140   Lorenz V. and Wanke H. (1979) The abundances of major, minor and trace elements in

1141   the earth's mantle as derived from primitive ultramafic nodules. *Proc. Lunar Planet. Sci.*

1142   *Conf. 10th*, 2031-2050.

1143 Jan M. Q. and Howie R. A. (1981) The Mineralogy and Geochemistry of the Metamorphosed

1144   Basic and Ultrabasic Rocks of the Jijal Complex, Kohistan, NW Pakistan. *J. Petrol.* **22**,

1145   85-126.

1146 Jochum K. P., Weis U., Stoll B., Kuzmin D., Yang Q., Raczek I., Jacob D. E., Stracke A.,

1147   Birbaum K., Frick D. A., Günther D. and Enzweiler J. (2011) Determination of reference

1148   values for NIST SRM 610-617 glasses following ISO guidelines. *Geostand.*

1149   *Geoanalytical Res.* **35**, 397-429.

Johan Z., Martin R. F. and Ettler V. (2017) Fluids are bound to be involved in the formation of ophiolitic chromite deposits. *Eur. J. Mineral.* **29**, 543-555.

Jousselin D. and Nicolas A. (2000) The Moho transition zone in the Oman ophiolite-relation with wehrlites in the crust and dunites in the mantle. *Mar. Geophys. Res.* **21**, 229-241.

Jousselin D., Nicolas A. and Boudier F. (1998) Detailed mapping of a mantle diapir below a paleo-spreading center in the Oman ophiolite. *J. Geophys. Res. Earth* **103**, 18153-18170.

Kelemen P. B. (1990) Reaction between ultramafic rock and fractionating basaltic magma I. phase relations, the origin of calc-alkaline magma series, and the formation of discordant dunite. *J. Petrol.* **31**, 51-98.

Kelemen P. B., Dick H. J. B. and Quick J. E. (1992) Formation of harzburgite by pervasive melt/rock reaction in the upper mantle. *Nature* **358**, 635-641.

Kelemen P. B., Hirth G., Shimizu N., Spiegelman M. and Dick H. J. (1997b) A review of melt migration processes in the adiabatically upwelling mantle beneath oceanic spreading ridges. *Philos. Trans. R. Soc. A Math. Phys. Eng. Sci.* **355**, 283-318.

Kelemen P. B., Koga K. and Shimizu N. (1997a) Geochemistry of gabbro sills in the crust-mantle transition zone of the Oman ophiolite: implications for the origin of the oceanic lower crust. *Earth Planet. Sci. Lett.* **146**, 475-488.

Kelemen P. B., Shimizu N. and Dunn T. (1993) Relative depletion of niobium in some arc magmas and the continental crust: partitioning of K, Nb, La and Ce during melt/rock reaction in the upper mantle. *Earth Planet. Sci. Lett.* **120**, 111-134.

Kelemen P. B., Shimizu N. and Salters V. J. M. (1995a) Extraction of mid-ocean-ridge basalt from the upwelling mantle by focused flow of melt in dunite channels. *Nature* **375**, 747-753.

Kelemen P. B., Whitehead J. A., Aharonov E. and Jordahl K. A. (1995b) Experiments on flow focusing in soluble porous media, with applications to melt extraction from the mantle. *J.*

1175   *Geophys. Res. Solid Earth* **100**, 475-496.

1176   Khedr M. Z., Arai S., Python M. and Tamura A. (2014) Chemical variations of abyssal

1177   peridotites in the central Oman ophiolite: Evidence of oceanic mantle heterogeneity.

1178   *Gondwana Res.* **25**, 1242-1262.

1179   Koga K. T., Kelemen P. B. and Shimizu N. (2001) Petrogenesis of the crust-mantle transition

1180   zone and the origin of lower crustal wehrlite in the Oman ophiolite. *Geochemistry,*

1181   *Geophys. Geosystems* **2**.

1182   Kogiso T., Tatsumi Y. and Nakano, S. (1997) Trace element transport during dehydration

1183   processes in the subducted oceanic crust: 1. Experiments and implications for the origin

1184   of ocean island basalts. *Earth Planet. Sci. Lett.* **148**, 193-205.

1185   Lanphere M. A. (1981) K-Ar ages of metamorphic rocks at the base of the Samail Ophiolite,

1186   Oman. *J. Geophys. Res. Solid Earth* **86**, 2777-2782.

1187   Leblanc M. and Ceuleneer G. (1991) Chromite crystallization in a multicellular magma flow:

1188   Evidence from a chromitite dike in the Oman ophiolite. *Lithos* **27**, 231-257.

1189   Lee C. T. A., Harbert A. and Leeman W. P. (2007) Extension of lattice strain theory to

1190   mineral/mineral rare-earth element partitioning: An approach for assessing

1191   disequilibrium and developing internally consistent partition coefficients between

1192   olivine, orthopyroxene, clinopyroxene and basaltic melt. *Geochim. Cosmochim. Acta* **71**,

1193   481-496.

1194   Lorand J. P. and Ceuleneer G. (1989) Silicate and base-metal sulfide inclusions in chromites

1195   from the Maqsad area (Oman ophiolite, Gulf of Oman): A model for entrapment. *Lithos*

1196   **22**, 173-190.

1197   MacLeod C. J., Johan Lissenberg C. and Bibby L. E. (2013) "Moist MORB" axial

1198   magmatism in the Oman ophiolite: The evidence against a mid-ocean ridge origin.

1199   *Geology* **41**, 459-462.

1200 Malvoisin B. (2015) Mass transfer in the oceanic lithosphere: Serpentinization is not
1201   isochemical. *Earth Planet. Sci. Lett.* **430**, 75-85.

1202 McKenzie D. and Bickle M. J. (1988) The volume and composition of melt generated by
1203   extension of the lithosphere. *J. Petrol.* **29**, 625-679.

1204 McKenzie D. and O'Nions R. K. (1991) Partial melt distribution from inversion of rare earth
1205   element concentrations. *J. Petrol.* **32**, 1021-1091.

1206 Le Mée L., Girardeau J. and Monnier C. (2004) Mantle segmentation along the Oman
1207   ophiolite fossil mid-ocean ridge. *Nature* **432**, 167-172.

1208 Monnier C., Girardeau J., Le Mée L. and Polvé M. (2006) Along-ridge petrological
1209   segmentation of the mantle in the Oman ophiolite. *Geochemistry, Geophys. Geosystems*
1210   **7**.

1211 Montigny R., Le Mer O., Thuizat R. and Whitechurch H. (1988) K-Ar and Ar study of
1212   metamorphic rocks associated with the Oman ophiolite: Tectonic implications.
1213   *Tectonophysics* **151**, 345-362.

1214 Moores E. M. and Vine F. J. (1971) The Troodos Massif, Cyprus and other Ophiolites as
1215   Oceanic Crust: Evaluation and Implications. *Philos. Trans. R. Soc. A Math. Phys. Eng.*
1216   *Sci.* **268**, 443-467.

1217 Navon O. and Stolper E. (1987) Geochemical consequences of melt percolation: the upper
1218   mantle as a chromatographic column. *J. Geol.* **95**, 285-307.

1219 Nicolas A., Bouldier F., Ildefonse B. and Ball E. (2000) Accretion of Oman and United Arab
1220   Emirates ophiolite - Discussion of a new structural map. *Mar. Geophys. Res.* **21**, 147-
1221   179.

1222 Nicolas A., Ceuleneer G., Boudier F. and Misseri M. (1988) Structural mapping in the Oman
1223   ophiolites: Mantle diapirism along an oceanic ridge. *Tectonophysics* **151**, 27-56.

1224 Nicolle M., Jousselin D., Reisberg L., Bosch D. and Stephant A. (2016) Major and trace

1225   element and Sr and Nd isotopic results from mantle diapirs in the Oman ophiolite:

1226   Implications for off-axis magmatic processes. *Earth Planet. Sci. Lett.* **437**, 138-149.

1227   Niu Y. (2004) Bulk-rock major and trace element compositions of abyssal peridotites:

1228   Implications for mantle melting, melt extraction and post-melting processes beneath

1229   Mid-Ocean ridges. *J. Petrol.* **45**, 2423-2458.

1230   O'Hara M. J. (1965) Primary magmas and the origin of basalts. *Scottish J. Geol.* **1**, 19–40.

1231   Ortoleva P., Chadam J., Merino E. and Sen A. (1987) Geochemical self-organization II: the

1232   reactive-infiltration instability. *Am. J. Sci.* **287**, 1008-1040.

1233   Palandri J. L. and Reed M. H. (2004) Geochemical models of metasomatism in ultramafic

1234   systems: Serpentinization, rodingitization, and sea floor carbonate chimney precipitation.

1235   *Geochim. Cosmochim. Acta* **68**, 1115-1133.

1236   Parkinson I. and Pearce J. (1998) Peridotites from the Izu-Bonin-Mariana Forearc (ODP Leg

1237   125): Evidence for mantle melting and melt-mantle interaction in a supra-subduction

1238   zone setting. *J. Petrol.* **39**, 1577-1618.

1239   Paulick H., Bach W., Godard M., De Hoog J. C. M., Suhr G. and Harvey J. (2006)

1240   Geochemistry of abyssal peridotites (Mid-Atlantic Ridge, 15°20'N, ODP Leg 209):

1241   Implications for fluid/rock interaction in slow spreading environments. *Chem. Geol.* **234**,

1242   179-210.

1243   Pearce J. A., Alabaster T., Shelton A. W. and Searle M. P. (1981) The Oman ophiolite as a

1244   Cretaceous arc-basin complex: evidence and implications. *Philos. Trans. R. Soc. London*

1245   **300**, 299-317.

1246   Prinzhofer A. and Allègre C. J. (1985) Residual peridotites and the mechanims of partial

1247   melting. *Earth Planet. Sci. Lett.* **74**, 251-265.

1248   Prinzhofer A., Nicolas A., Cassard D., Moutte J., Leblanc M., Paris J. P. and Rabinovitch M.

1249   (1980) Structures in the new caledonia peridotites-gabbros: Implications for oceanic

mantle and crust. *Tectonophysics* **69**, 85-112.

Python M. and Ceuleneer G. (2003) Nature and distribution of dykes and related melt migration structures in the mantle section of the Oman ophiolite. *Geochemistry, Geophys. Geosystems* **4**.

Python M., Ceuleneer G. and Arai S. (2008) Chromian spinels in mafic-ultramafic mantle dykes: Evidence for a two-stage melt production during the evolution of the Oman ophiolite. *Lithos* **106**, 137-154.

Python M., Ceuleneer G., Ishida Y., Barrat J.-A. and Arai S. (2007) Oman diopsidites: a new lithology diagnostic of very high temperature hydrothermal circulation in mantle peridotite below oceanic spreading centres. *Earth Planet. Sci. Lett.* **255**, 289-305.

Python M., Yoshikawa M., Shibata T. and Arai S. (2011) Diopsidites and Rodingites: Serpentinisation and Ca-Metasomatism in the Oman Ophiolite Mantle. In *Dyke Swarms: Keys for Geodynamic Interpretations* Springer Berlin Heidelberg, Berlin, Heidelberg. pp. 401-435.

Quick J. E. (1981) Petrology and petrogenesis of the Trinity Peridotite, an upper mantle diapir in the Eastern Klamath Mountains, Northern California. *J. Geophys. Res.* **86**, 11837-11863.

Rabinowicz M. and Ceuleneer G. (2005) The effect of sloped isotherms on melt migration in the shallow mantle: a physical and numerical model based on observations in the Oman ophiolite. *Earth Planet. Sci. Lett.* **229**, 231-246.

Rabinowicz M., Ceuleneer G. and Nicolas A. (1987) Melt segregation and flow in mantle diapirs below spreading centres: evidence from the Oman ophiolite. *J. Geophys. Res.* **92**, 3475-3486.

Rampone E., Borghini G., Godard M., Ildefonse B., Crispini L. and Fumagalli P. (2016) Melt/rock reaction at oceanic peridotite/gabbro transition as revealed by trace element

1275   chemistry of olivine. *Geochim. Cosmochim. Acta* **190**, 309-331.

1276 Rioux M., Bowring S., Kelemen P., Gordon S., Dudás F. and Miller R. (2012) Rapid crustal

1277   accretion and magma assimilation in the Oman-U.A.E. ophiolite: High precision U-Pb

1278   zircon geochronology of the gabbroic crust. *J. Geophys. Res. Solid Earth* **117**.

1279 Rospabé M. (2018) Etude pétrologique, géochimique et structurale de la zone de transition

1280   dunitique dans l'ophiolite d'Oman: Identification des processus pétrogénétiques à

1281   l'interface manteau/croûte. *PhD thesis* Université Toulouse III - Paul Sabatier.

1282 Rospabé M., Benoit M. and Candaudap F. (2018) Determination of Trace Element Mass

1283   Fractions in Ultramafic Rocks by HR-ICP-MS: A Combined Approach Using a Direct

1284   Digestion/Dilution Method and Pre-concentration by Co-precipitation. *Geostand.*

1285   *Geoanalytical Res.* **42**, 115-129.

1286 Rospabé M., Ceuleneer G., Benoit M., Abily B. and Pinet P. (2017) Origin of the dunitic

1287   mantle-crust transition zone in the Oman ophiolite: The interplay between percolating

1288   magmas and high-temperature hydrous fluids. *Geology* **45**, 471-474.

1289 Sanfilippo A., Dick H. J. B. and Ohara Y. (2013) Melt-rock reaction in the mantle: Mantle

1290   troctolites from the parecevela ancient back-arc spreading center. *J. Petrol.* **54**, 861-885.

1291 Sanfilippo A., Morishita T., Kumagai H., Nakamura K., Okino K., Hara K., Tamura A. and

1292   Arai S. (2015) Hybrid troctolites from mid-ocean ridges: Inherited mantle in the lower

1293   crust. *Lithos* **232**, 124-130.

1294 Sanfilippo A. and Tribuzio R. (2013a) Building of the deepest crust at a fossil slow-spreading

1295   centre (Pineto gabbroic sequence, Alpine Jurassic ophiolites). *Contrib. to Mineral.*

1296   *Petrol.* **165**, 705-721.

1297 Sanfilippo A. and Tribuzio R. (2013b) Origin of olivine-rich troctolites from the oceanic

1298   lithosphere: A comparison between the Alpine Jurassic ophiolites and modern slow

1299   spreading ridges. *Ofioliti* **38**, 89-99.

1300 Sanfilippo A., Tribuzio R., Ottolini L. and Hamada M. (2017) Water, lithium and trace
1301   element compositions of olivine from Lanzo South replacive mantle dunites (Western
1302   Alps): New constraints into melt migration processes at cold thermal regimes. *Geochim.*
1303   *Cosmochim. Acta* **214**, 51-72.

1304 Sanfilippo A., Tribuzio R. and Tiepolo M. (2014) Mantle–crust interactions in the oceanic
1305   lithosphere: Constraints from minor and trace elements in olivine. *Geochim. Cosmochim.*
1306   *Acta* **141**, 423-439.

1307 Savov I. P., Ryan J. G., D'Antonio M., Kelley K. and Mattie P. (2005) Geochemistry of
1308   serpentinized peridotites from the Mariana Forearc Conical Seamount, ODP Leg 125:
1309   Implications for the elemental recycling at subduction zones. *Geochemistry, Geophys.*
1310   *Geosystems* **6**.

1311 Schiano P., Clocchiatti R., Lorand J.-P., Massare D., Deloule E. and Chaussidon M. (1997)
1312   Primitive basaltic melts included in podiform chromites from the Oman Ophiolite. *Earth*
1313   *Planet. Sci. Lett.* **146**, 489-497.

1314 Snow J. E. and Dick H. J. B. (1995) Pervasive magnesium loss by marine weathering of
1315   peridotite. *Geochim. Cosmochim. Acta* **59**, 4219-4235.

1316 Sobolev A. (1996) Melt Incusions in Minerals as a source of princple petrological
1317   information. *Petrology* **4**, 209-220.

1318 Stead C. V., Tomlinson E. L., McKenna C. A. and Kamber B. S. (2017) Rare earth element
1319   partitioning and subsolidus exchange behaviour in olivine. *Chem. Geol.* **475**, 1-13.

1320 Suhr G., Kelemen P. and Paulick H. (2008) Microstructures in Hole 1274A peridotites, ODP
1321   Leg 209, Mid-Atlantic Ridge: Tracking the fate of melts percolating in peridotite as the
1322   lithosphere is intercepted. *Geochemistry, Geophys. Geosystems* **9**.

1323 Sun C. and Liang Y. (2014) An assessment of subsolidus re-equilibration on REE distribution
1324   among mantle minerals olivine, orthopyroxene, clinopyroxene, and garnet in peridotites.

1325   *Chem. Geol.* **372**, 80-91.

1326   Sun S.-S. and McDonough W. F. (1989) Chemical and isotopic systematics of oceanic

1327   basalts: implications for mantle composition and processes. *Geol. Soc. London, Spec.*

1328   *Publ.* **42**, 313-345.

1329   Sundberg M., Hirth G. and Kelemen P. B. (2010) Trapped melt in the Josephine peridotite:

1330   Implications for permeability and melt extraction in the upper mantle. *J. Petrol.* **51**, 185-

1331   200.

1332   Takazawa E., Okayasu T. and Satoh K. (2003) Geochemistry and origin of the basal

1333   lherzolites from the northern Oman ophiolite (northern Fizh block). *Geochemistry,*

1334   *Geophys. Geosystems* **4**.

1335   Tamura A., Morishita T., Ishimaru S. and Arai S. (2014) Geochemistry of spinel-hosted

1336   amphibole inclusions in abyssal peridotite: Insight into secondary melt formation in

1337   melt-peridotite reaction. *Contrib. to Mineral. Petrol.* **167**, 1-16.

1338   Tilley C. E., Thompson R. N. and Lovenbury P. A. (2007) Melting relations of some oceanic

1339   basalts. *Geol. J.* **8**, 59-64.

1340   Tilton G. R., Hopson C. A. and Wright J. E. (1981) Uranium-lead isotopic ages of the Samail

1341   Ophiolite, Oman, with applications to Tethyan ocean ridge tectonics. *J. Geophys. Res.*

1342   *Solid Earth* **86**, 2763-2775.

1343   Tippit P. R., Pessagno J. E. A. and Smewing J. D. (1981) The biostratigraphy of sediments in

1344   the volcanic unit of the Samail ophiolite. *J. Geophys. Researc* **86**, 2756-2762.

1345   Toramaru A. and Fujii N. (1986) Connectivity of melt phase in a partially molten peridotite.

1346   *J. Geophys. Res. Solid Earth* **91**, 9239-9252.

1347   Van Orman J. A., Grove T. L. and Shimizu N. (2001) Rare earth element diffusion in

1348   diopside: influence of temperature, pressure, and ionic radius, and an elastic model for

1349   diffusion in silicates. *Contrib. to Mineral. Petrol.* **141**, 687-703.

1350   Verhoogen J. (1954) Petrological evidence on temperature distribution in the mantle of the

1351   earth. *Eos, Trans. Am. Geophys. Union.*

1352   Vernières J., Godard M. and Bodinier J.-L. (1997) A plate model for the simulation of trace

1353   element fractionation during partial melting and magma transport in the Earth's upper

1354   mantle. *J. Geophys. Res.* **102**, 24771.

1355   Yamasaki T., Maeda J. and Mizuta T. (2006) Geochemical evidence in clinopyroxenes from

1356   gabbroic sequence for two distinct magmatisms in the Oman ophiolite. *Earth Planet. Sci.*

1357   *Lett.* **251**, 52-65.

1358   Yokoyama T., Makishima A. and Nakamura E. (1999) Evaluation of the coprecipitation of

1359   incompatible trace elements with fluoride during silicate rock dissolution by acid

1360   digestion. *Chem. Geol.* **157**, 175-187.

1361   You C. F., Castillo P. R., Gieskes J. M., Chan L. H. and Spivack, A. J. (1996) Trace element

1362   behavior in hydrothermal experiments: Implications for fluid processes at shallow depths

1363   in subduction zones. *Earth Planet. Sci. Lett.* **140**, 41-52.
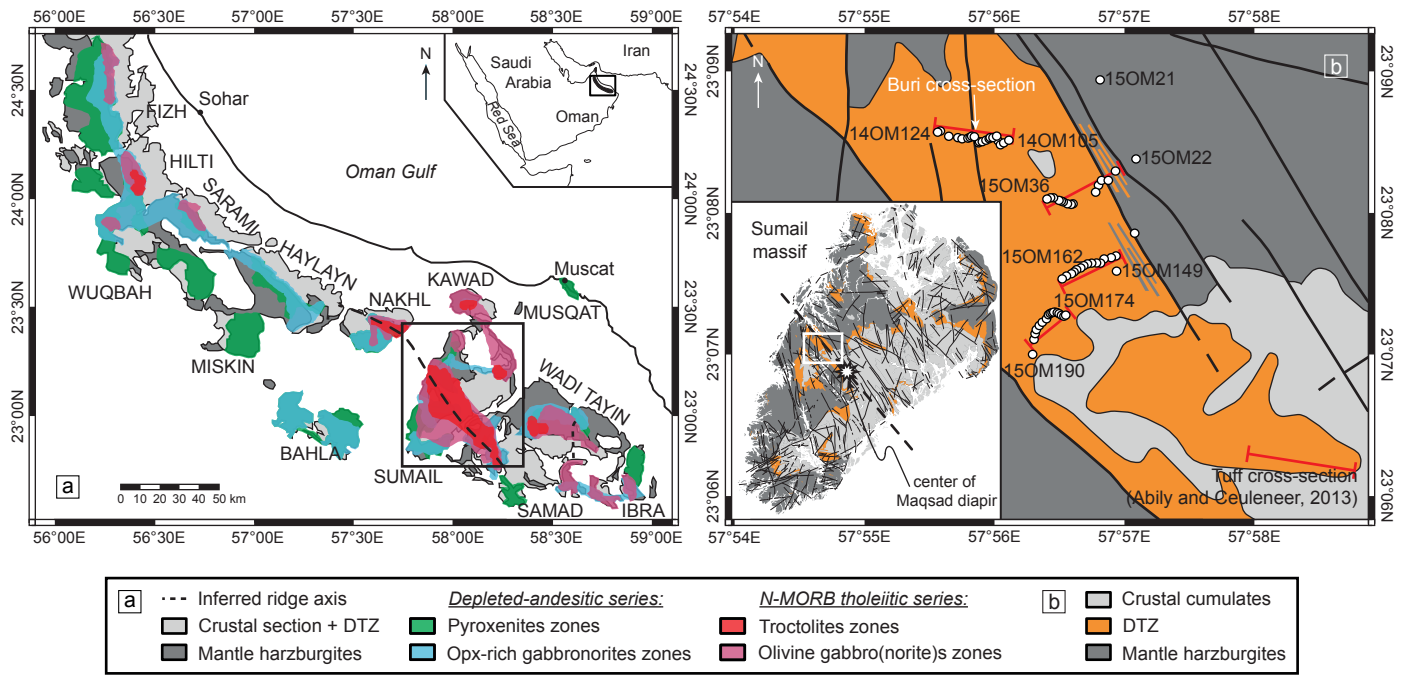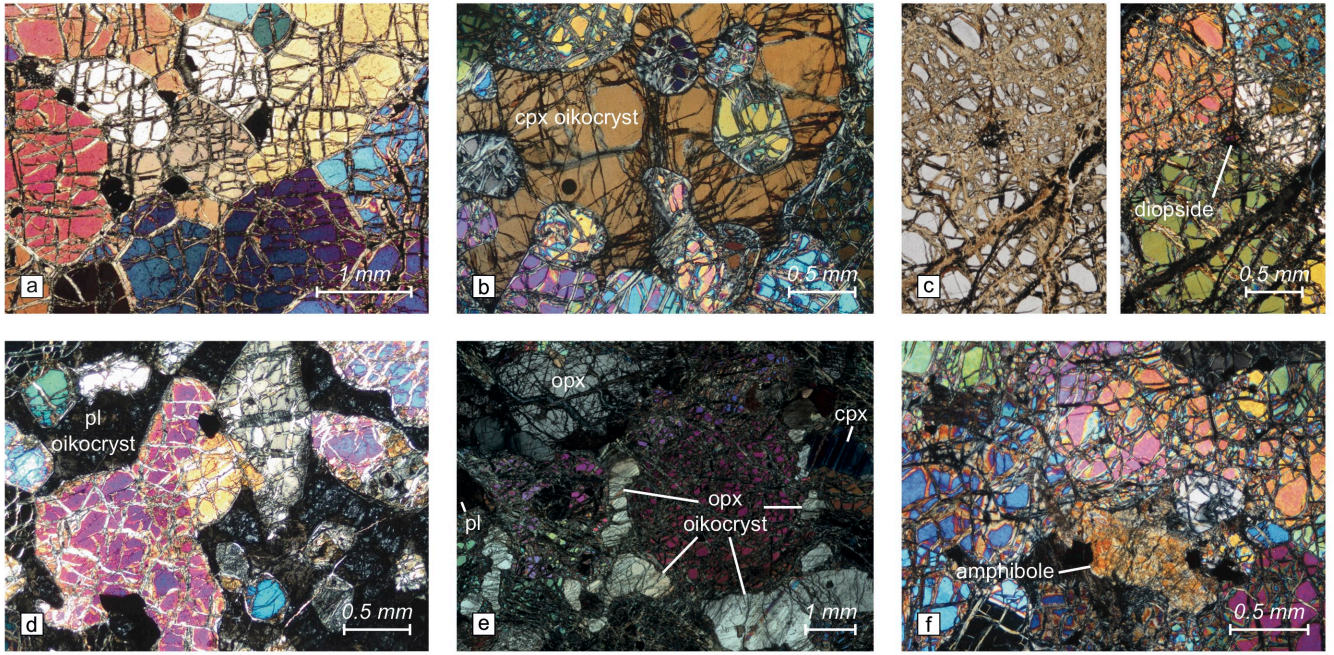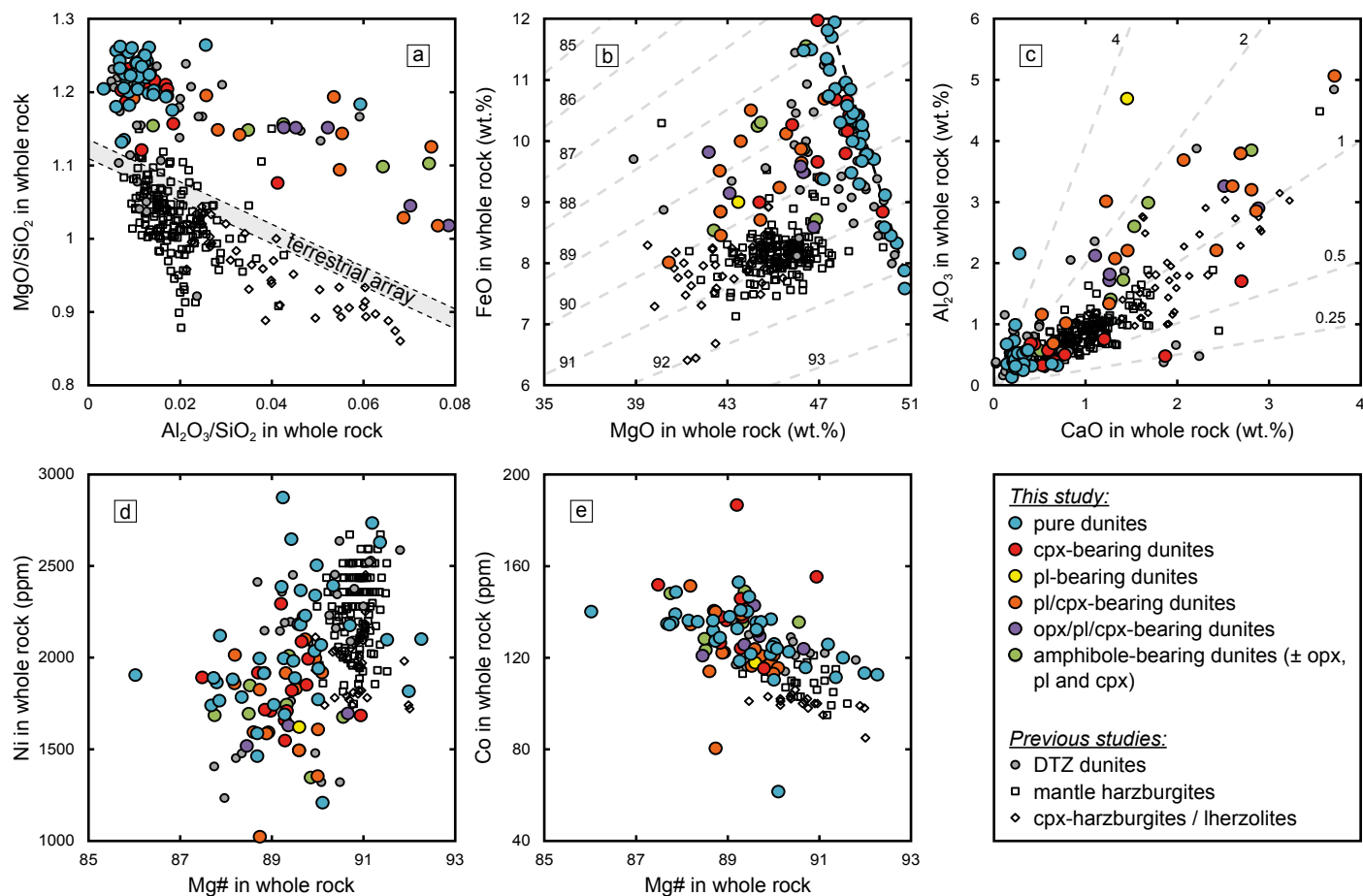
Figure 1

Figure 2

Figure 3

Figure 4

This study:
- pure dunites (light blue)
- cpx-bearing dunites (red)
- pl-bearing dunites (yellow)
- pl/cpx-bearing dunites (orange)
- opx/pl/cpx-bearing dunites (purple)
- amphibole-bearing dunites (± opx, pl and cpx) (green)
- diopside in all types of dunite (dark blue)

Previous studies:
- DTZ dunites (grey)
- mantle harzburgites (open square)
- cpx-harzburgites / lherzolites (open diamond)
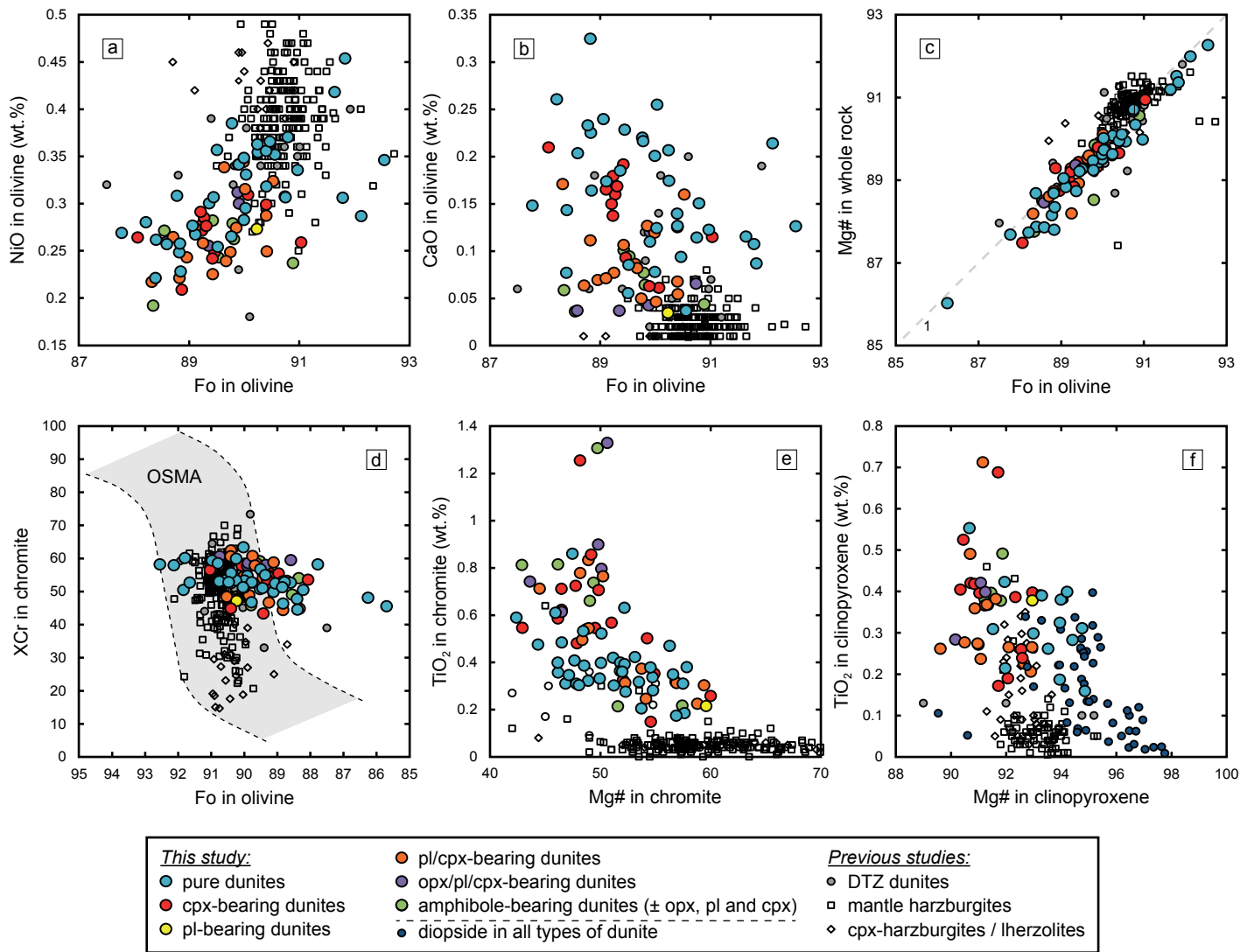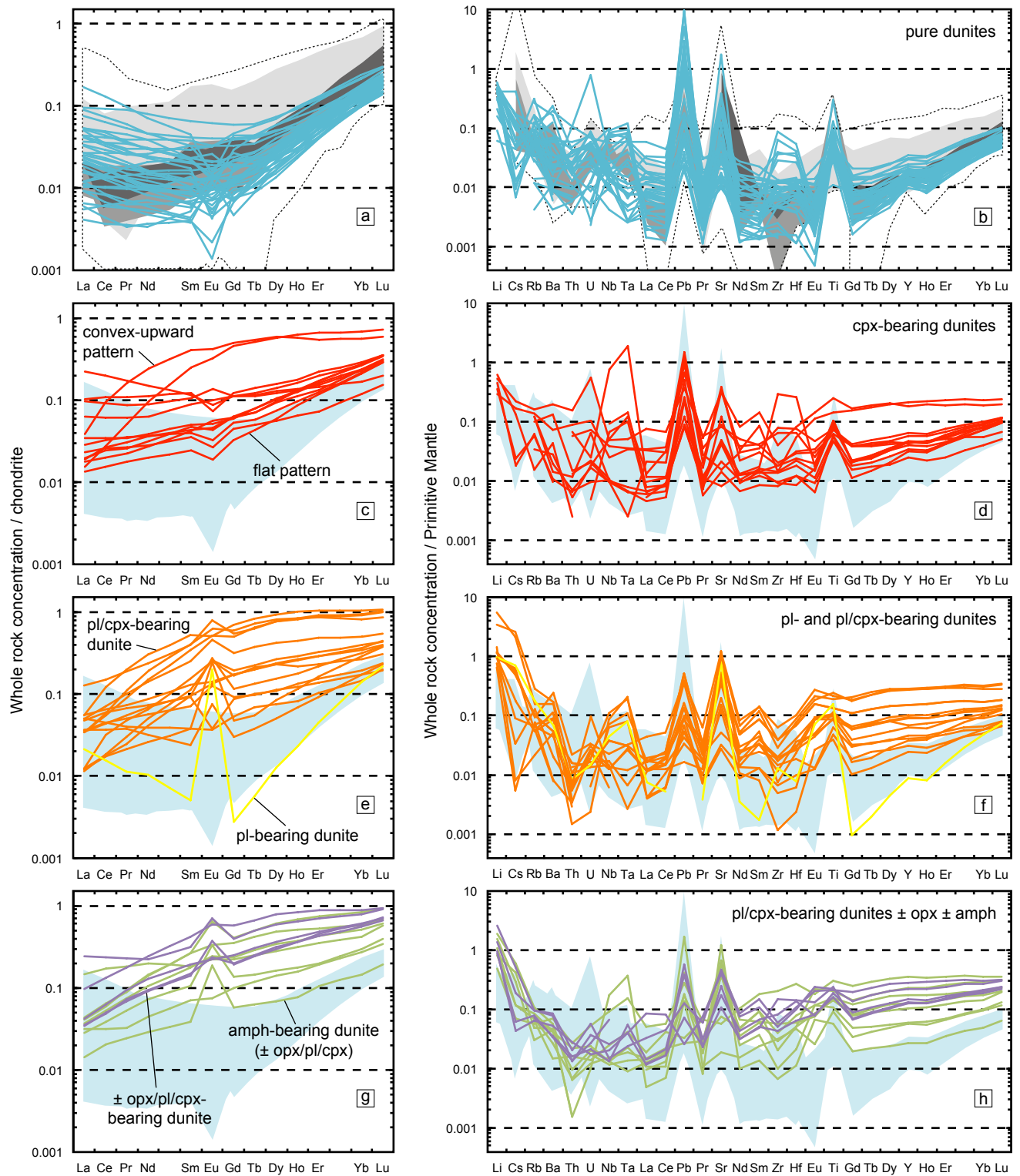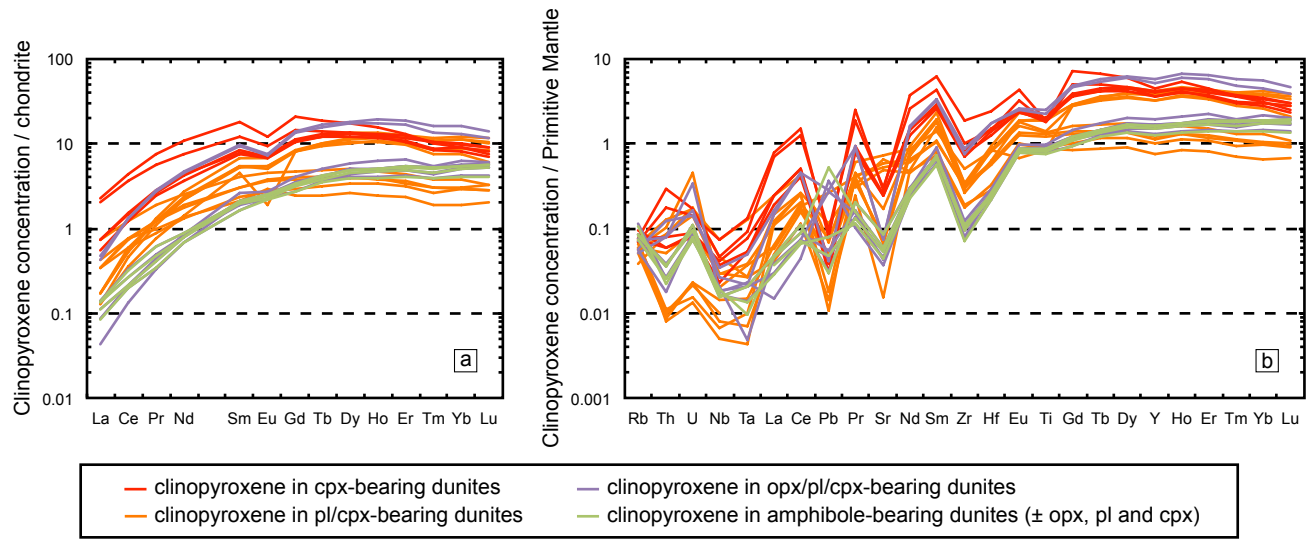
Figure 5

Figure 6

Figure 7

Figure 8

Figure 9

Legend:

This study:
- calculated melts in equilibrium with clinopyroxene (colours refer to the facies of the host rock)
- averaged melt in equilibrium with clinopyroxene used in models (Appendix C)

Previous studies:
- V1 lavas
- V2t1 lavas
- V2t2 lavas
- boninite
- N-MORB

Panel labels:
- a: MORB-type melts (La_{CN}/Yb_{CN} ~0.48)
- b: LREE-enriched melts (La_{CN}/Yb_{CN} ~1.50)
- c: LREE-depleted melts (La_{CN}/Yb_{CN} ~0.16)

Y-axis: Concentration / chondrite

X-axis elements: La Ce Pr Nd Sm Eu Gd Tb Dy Ho Er Tm Yb Lu

Figure 10